

REPORT 1295

AN ANALYSIS OF ONCE-PER-REVOLUTION OSCILLATING AERODYNAMIC THRUST LOADS ON SINGLE-ROTATION PROPELLERS ON TRACTOR AIRPLANES AT ZERO YAW¹

By VERNON L. ROGALLO, PAUL F. YAGGY, and JOHN L. MCCLOUD III

SUMMARY

A simplified procedure is shown for calculating the once-per-revolution oscillating aerodynamic thrust loads on propellers of tractor airplanes at zero yaw. The only flow field information required for the application of the procedure is a knowledge of the upflow angles at the horizontal center line of the propeller disk. Methods are presented whereby these angles may be computed without recourse to experimental survey of the flow field.

The loads computed by the simplified procedure are compared with those computed by a more rigorous method and the procedure is applied to several airplane configurations which are believed typical of current designs. The results are generally satisfactory.

INTRODUCTION

An important consideration in the structural design of propellers is that which deals with vibratory stresses resulting from the blade bending flatwise 1 cycle per propeller revolution (hereafter referred to as 1-*P* stresses). This flatwise bending of the propeller blade is due primarily to aerodynamic thrust loads oscillating 1 cycle per propeller revolution (hereafter referred to as 1-*P* thrust loads) which are imposed on the blade as a result of propeller thrust-axis inclination and/or asymmetries of the flow fields in which the propellers operate.

Methods have been developed whereby these 1-*P* stresses have been computed satisfactorily for isolated propellers (e. g., refs. 1 and 2). These methods assumed a uniform flow field at the propeller disk, that is, the flow of air into the propeller disk was assumed to be at a uniform speed and stream angle at all points on the disk. However, for cases of propellers operating in nonuniform flow fields of wing-nacelle-fuselage combinations, the validity of these assumptions was in question and it was not known to what degree the values thus computed would agree with those measured.

In considering where errors might possibly arise in computing the 1-*P* stresses when the flow field is nonuniform, it should be pointed out that prediction of the 1-*P* stresses requires a knowledge of the 1-*P* thrust loads and the structural properties of the propeller. In turn, methods of computing the 1-*P* thrust loads require a knowledge of the flow-field characteristics, the blade physical properties (airfoil section, plan form, etc.) and the blade aerodynamic properties (two-dimensional). Finally, methods of computing the flow-field characteristics require taking proper

account of the influence of the various airplane components and their interference effects on each other.

It was recognized that the blade structural, geometric, and aerodynamic characteristics did not depend upon the uniformity of the flow field; however, sources of error might possibly lie in the answers to one or more of the following questions.

(1) If the 1-*P* aerodynamic thrust load is known, can the 1-*P* stresses be computed?

(2) If (1) can be accomplished, can the 1-*P* thrust loads be computed if the flow-field characteristics are known?

(3) If numbers (1) and (2) can be accomplished, can the flow field characteristics be computed for any given airplane configuration?

To answer the above questions, an analysis of the methods employed to obtain 1-*P* blade stresses, 1-*P* thrust loads, and flow-field parameters was undertaken. An investigation of a propeller operating in the nonuniform flow field of a wing-nacelle-fuselage combination was made in the Ames 40- by 80-foot wind tunnel. The data obtained from this investigation were reported in references 3 and 4. These data consisted of surveys of the flow field in the absence of the propeller, measurements of stresses on the propeller blades operating in this flow field, and surveys of the wake pressures behind the operating propeller. During the analysis of these data, a simplification was devised whereby the 1-*P* thrust loads could be computed by a method requiring only a knowledge of the upflow angles at the horizontal center line of the propeller disk. Efforts were then directed toward developing methods whereby these upflow angles could be computed without recourse to experimental survey (these surveys had proved to be quite tedious and cumbersome). The methods which were developed were presented in references 5, 6, and 7. To evaluate the adequacy of these methods, it was necessary to obtain additional experimental flow-field information on different wing-nacelle-fuselage combinations. The results of the surveys at the propeller planes of six model configurations tested in the Ames 40- by 80-foot wind tunnel were reported in reference 8. Mach number effects on the upflow angles were investigated to a Mach number of 0.92 by Messrs. Lopez and Dickson in the Ames 12-foot wind tunnel. These results were reported in reference 9.

This report presents an analysis, based on the information in references 3 through 9, of the problem of computing 1-*P* stresses for propellers operating in nonuniform flow fields.

¹ Supersedes NACA TN 3395 entitled "On the Calculation of the 1-*P* Oscillating Aerodynamic Loads on Single-Rotation Propellers in Pitch on Tractor Airplanes," by Vernon L. Rogallo and Paul F. Yaggy, 1955.

NOTATION

c_t	blade-section thrust coefficient, $\frac{t}{\rho n_p^2 D^4}$
c_{t_l}	blade-section thrust coefficient due to blade-section lift force only, $\frac{\text{section thrust due to lift}}{\rho n_p^2 D^4}$
D	propeller diameter, ft
$\frac{d\epsilon}{d\alpha}$	upwash parameter, rate of change of upwash with angle of attack
n_p	propeller rotational speed, revolutions per second except where otherwise noted
R	propeller radius, ft
r	distance along any radial line from the propeller thrust axis, ft
t	blade-section thrust, lb
V_∞	free-stream velocity, feet per second except where otherwise noted
V'	component of the local velocity in the plane perpendicular to a radial line (see fig. 1), ft/sec
V_B	resultant velocity acting on any blade section, neglecting propeller-induced effects, ft/sec
V_t	local velocity at any point (r, Ω) at the propeller plane, ft/sec
x	radial location of any blade section, $\frac{r}{R}$

$1-P$	the fundamental component (1 cycle per propeller revolution) of the oscillation of the blade-section thrust coefficient or of the vibratory blade stresses
α	angle of attack of a wing or a body relative to the free-stream velocity measured at the plane of symmetry, deg
α_G	geometric angle of attack of the thrust axis relative to the free-stream velocity, deg
β_x	section blade angle at radial station x , deg
δc_{t_l}	amplitude of the $1-P$ component of the variation of incremental section thrust coefficient due to section lift force, further defined as the $1-P$ aerodynamic thrust load
Δc_t	incremental section-thrust coefficient, $c_{t\Omega} - c_{t\Omega=0}$
Δc_{t_l}	incremental section-thrust coefficient due to section lift force, $c_{t_l\Omega} - c_{t_l\Omega=0}$
ϵ	angle of upwash, measured from a line parallel to the free-stream direction in a plane parallel to the model plane of symmetry, deg
η	spanwise station from the longitudinal center line of a wing, semispans
θ	angle of outflow, measured from a line parallel to the thrust axis in a plane through the thrust axis (see fig. 1)
θ'	angle at which the local velocity at any point on

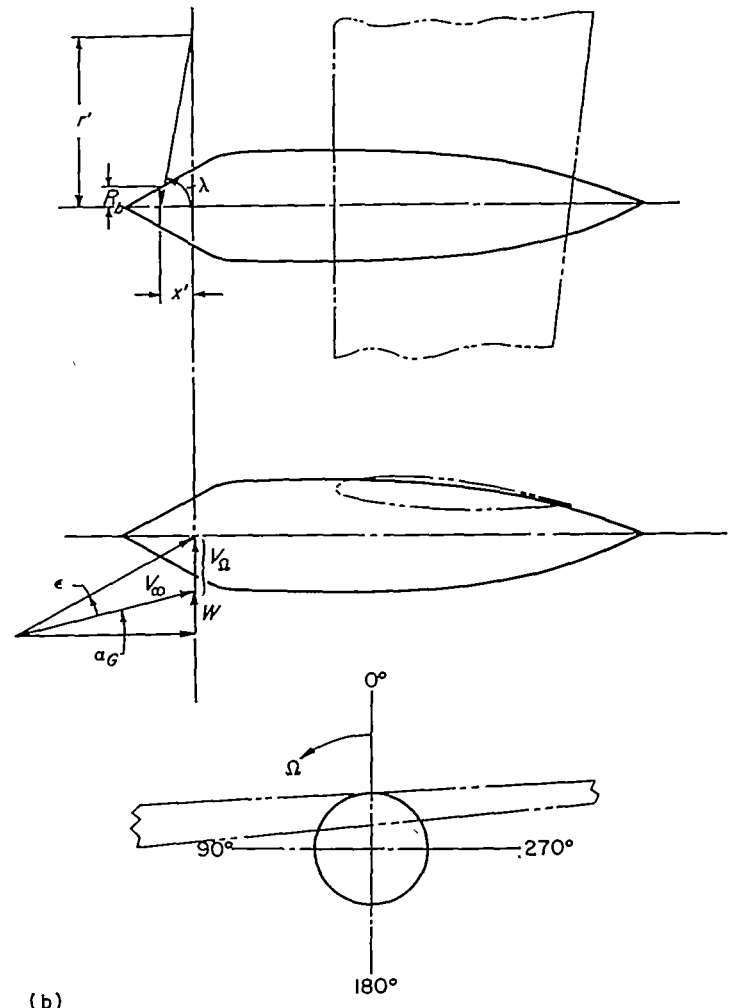


FIGURE 1.—Geometric characteristics of the flow parameters relative to the survey disk. All angles and vectors shown positive.

the propeller disk is inclined to the plane perpendicular to the radial line through that point (see fig. 1)

- Λ sweep angle of the wing quarter-chord line, positive for sweepback
- Λ_β effective wing sweep for compressible flow ($\Lambda_\beta = \tan^{-1}(\tan \Lambda)/\beta$)
- ρ mass density of the air in the free stream, slugs/cu ft
- φ_a phase angle between the position of the maximum 1-P magnitude and the $\Omega=90^\circ$ position, deg
- ψ angle of rotational flow (an apparent, not an actual rotation) measured from a line parallel to the thrust axis in a plane perpendicular to a radial line (see fig. 1), deg
- Ω angular position about the thrust axis, measured counterclockwise from the upper vertical position as seen from the front, deg

SUBSCRIPTS

- T total effects resulting from consideration of variations in ψ , θ , and $\frac{V_1}{V_\infty}$ acting simultaneously
- $\theta, \frac{V_1}{V_\infty}$ effects resulting from consideration of variations in θ and $\frac{V_1}{V_\infty}$ only
- ψ effects resulting from consideration of variations in ψ only

RESULTS AND DISCUSSION

COMPUTATION OF THE 1-P STRESSES FROM KNOWN 1-P AERODYNAMIC THRUST LOADS

A method for computing the 1-P vibratory stresses on a propeller blade using known 1-P thrust loads has been developed and presented in reference 10. Although this method has been proven to be adequate for isolated propellers operating in uniform flow fields, its accuracy for propellers operating in nonuniform flow fields has not been established. An evaluation of this method was undertaken for a typical wing-nacelle-fuselage combination. Wind-tunnel tests of the combination were made in the Ames 40- by 80-foot wind tunnel to provide the necessary experimental data. The propeller stresses were measured on the blades by means of strain gages. Simultaneously, the variations of the aerodynamic thrust loads were measured by means of total-head pressure rakes mounted in the propeller slip-stream as shown in figure 2. From the variations thus obtained, the 1-P components of both the vibratory stresses and the oscillatory thrust loads were extracted by conventional wave-form analysis.

A typical radial variation of the double amplitude of the 1-P thrust load is shown for a blade angle of 20° at $0.75R$ in figure 3. By use of these measured 1-P thrust loads, 1-P stresses were calculated and are compared with the measured 1-P stresses in figure 4. (Also shown in fig. 4 is a similar comparison for another blade angle.) Good agreement is indicated which is interpreted as verifying that the

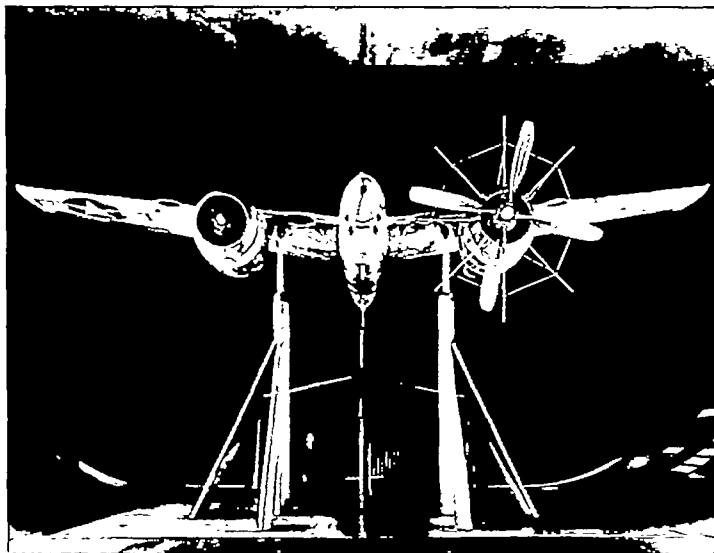


FIGURE 2.—Twin-engine airplane mounted in the Ames 40- by 80-foot wind tunnel showing propeller and wake survey instrumentation.

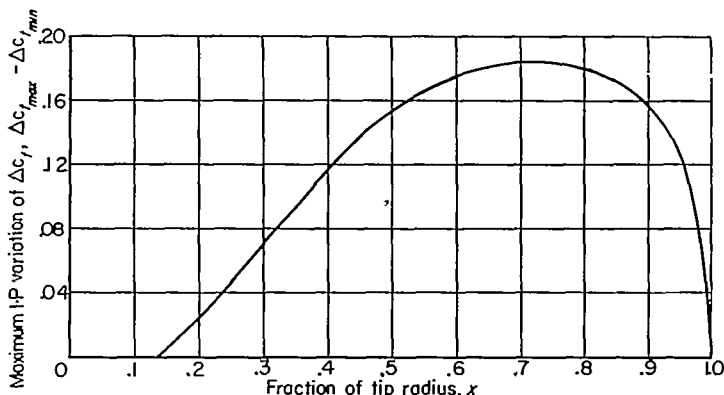


FIGURE 3.—Measured radial variation of the maximum 1-P incremental thrust coefficient; $V_\infty=165$ mph, $n_p=1250$ rpm, $\alpha_G=8^\circ$, $\beta_{0.75}=20^\circ$, four-blade propeller.

1-P stresses in a propeller operating in a nonuniform flow field can be computed if the 1-P thrust load is known.

COMPUTATION OF THE 1-P AERODYNAMIC THRUST LOAD FROM KNOWN FLOW-FIELD CHARACTERISTICS

A method utilizing strip analysis to compute the thrust load variation from known flow-field characteristics has been developed and is presented in Appendix A. An evaluation of the method was undertaken for propellers in nonuniform flow fields by attempting to compute the 1-P thrust loads measured during the tests of the wing-nacelle-fuselage combination shown in figure 2.

The flow-field characteristics required for this wing-nacelle-fuselage combination were obtained by surveying the flow field at the plane of the propeller in the absence of the propeller. A rake of eight directional pitot-static tubes (described in ref. 3) was employed for the survey. The flow field was defined by three parameters; the rotational flow angle, ψ , the outflow angle, θ , and the velocity ratio, V_1/V_∞ , all of which are defined in the Notation and shown in figure 1. Typical variations of these parameters with

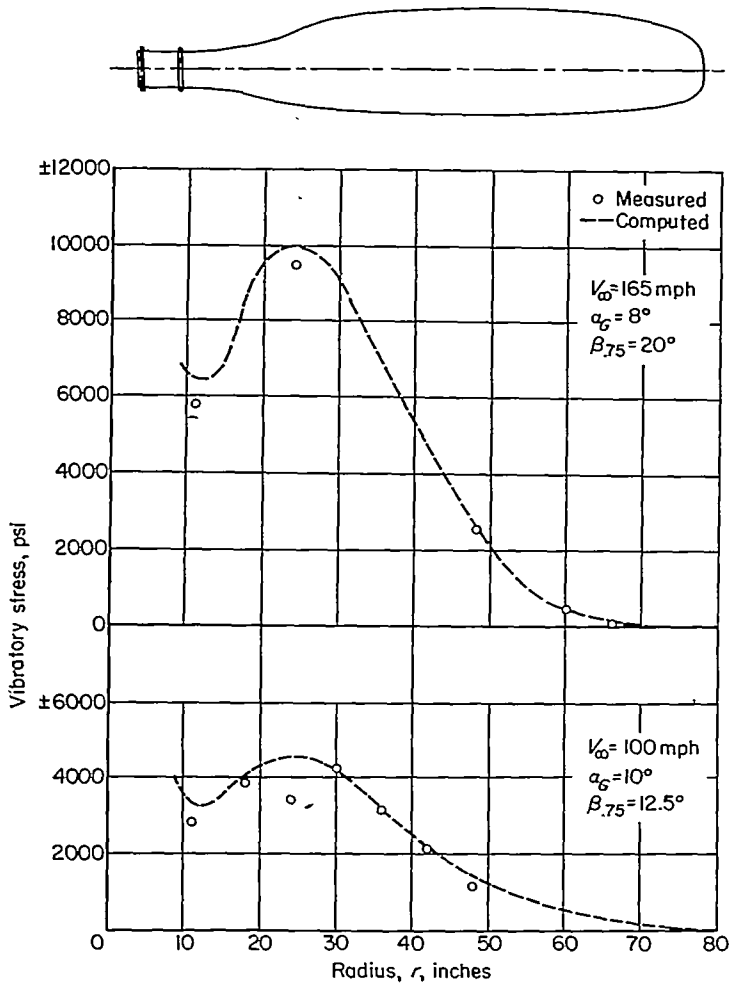
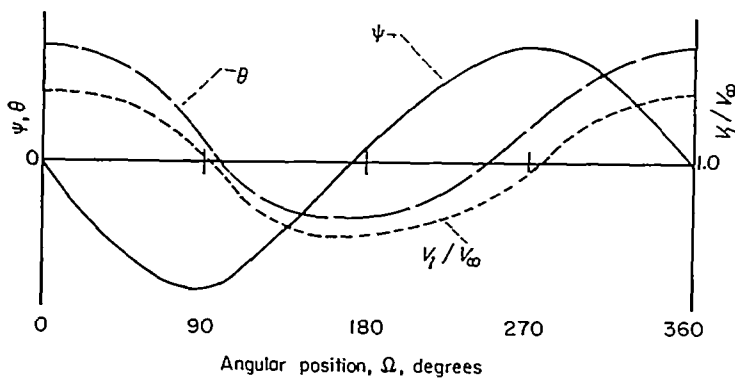
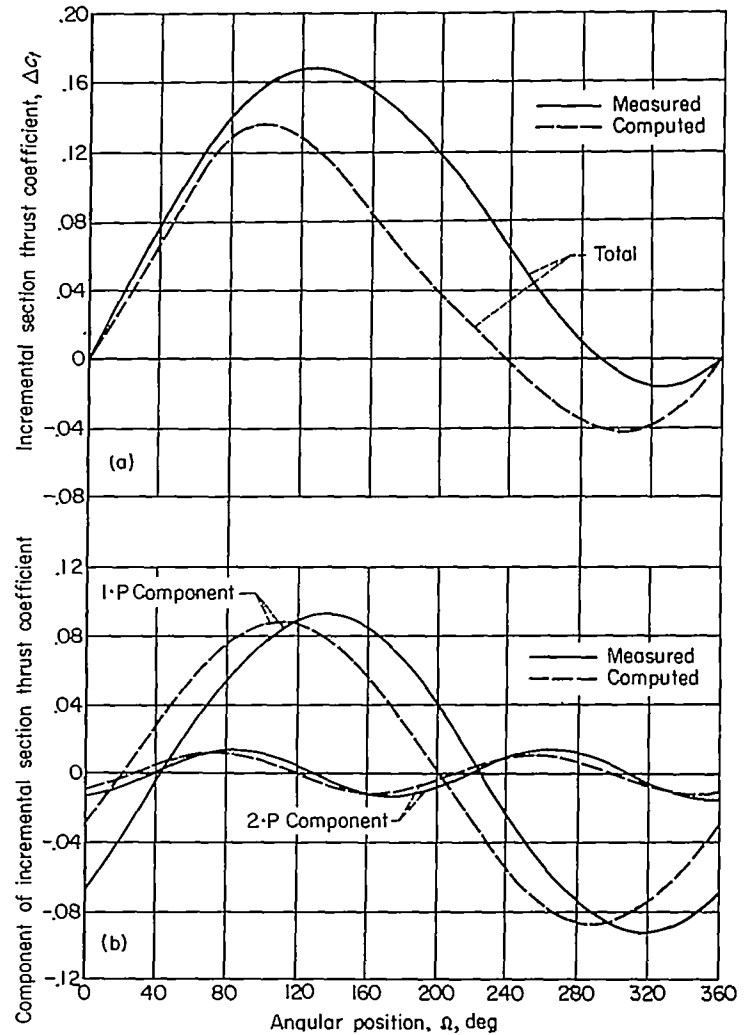


FIGURE 4.—Comparison of computed and measured stress distributions for a four-blade propeller.

angular position about the thrust axis are shown in the following sketch.



From the measured flow-field parameters, the variation of the total aerodynamic thrust load was computed by the method described in Appendix A. In figure 5(a), the computed variation is compared with that measured by the thrust rake for a typical case at the 0.7 radius of the propeller. The adequacy of the method is demonstrated by the agreement of both the absolute magnitude and the wave forms of the variations. The phase angle between the variations is of no consequence to the problem of computing the 1-P stresses; it resulted primarily from rotation of the slipstream before it reached the thrust rake.



(a) Variation of the total incremental thrust coefficient.

(b) Variation of the 1-P and 2-P components.

FIGURE 5.—Comparison of computed and measured section thrust-coefficient variations at the 0.7-radius station of the propeller; $V_\infty = 165$ mph, $\alpha_G = 8^\circ$, $n_p = 1250$ rpm, $\beta_{0.75} = 20^\circ$, four-blade propeller.

From the variations shown in figure 5(a), the 1-P and 2-P oscillatory components² were separated and are compared in figure 5(b). Again, aside from the phase shift, good agreement between measured and computed values is indicated. Similar accuracy was realized for all radial positions on the propeller blade as is indicated in figure 6 by a comparison of the variation of the 1-P thrust load with radial position as measured and as computed.

To obtain the accuracy indicated in figures 5 and 6 in computing the 1-P thrust loads, it was necessary to compute, using the measured flow-field data, the variation of the total aerodynamic thrust load at at least 16 angular positions for each radial position. This, in turn, required an accurate knowledge of the flow-field parameters at these angular positions. If this information is available, and the limitations set forth in Appendix A are not exceeded, it is concluded that the 1-P thrust load can be computed from known flow-field characteristics.

² No other harmonic components of appreciable amplitude were found to be present.

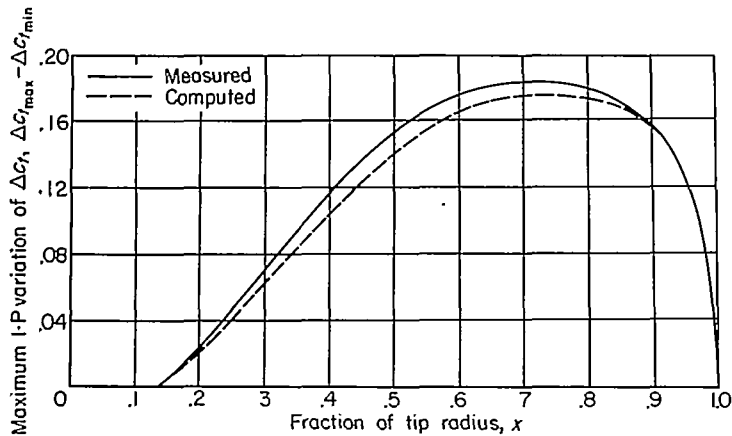


FIGURE 6.—Comparison of the computed and measured distributions of the maximum variations of the 1-P incremental section thrust coefficient; $V_\infty=165$ mph, $n_p=1250$ rpm, $\alpha_d=8^\circ$, $\beta_{0.75}=20^\circ$, four-blade propeller.

COMPUTATION OF THE FLOW-FIELD CHARACTERISTICS FOR ANY GIVEN AIRPLANE CONFIGURATION

On the basis of the results given previously, it appears that predictions of the 1-P stresses depend on an accurate knowledge of certain flow-field characteristics which can be obtained by sufficiently extensive experimental surveys of the flow field at the propeller plane. These surveys are quite laborious and it would be desirable to be able to compute the required flow parameters. It was found that no known methods for computing all the flow-field parameters were available and attempts to develop such methods posed formidable problems whose solutions were not readily apparent. Therefore, rather than attempting to approach this problem directly, an attempt was made to consider the influence of each of the flow-field parameters on the 1-P thrust load; the prime purpose being to discover simplifications which could be accepted in determining the amplitude of the 1-P thrust load.

The variation of the oscillating aerodynamic thrust load on a blade element was calculated by equation (A7), Appendix A, using measured flow-field parameters at 16 angular positions. Three cases were investigated; namely,

- (1) The use of measured values of ψ with the assumption that $\theta=0^\circ$, and $V_i/V_\infty=1.0$
- (2) The use of measured values of θ and V_i/V_∞ with the assumption that $\psi=0^\circ$
- (3) The use of measured values of ψ , θ , and V_i/V_∞

From the variations thus obtained, the 1-P components were extracted.

From figure 1, it is seen that the first case shows the effect of variations in the direction of the vector V' and the second case shows the effect of variations in the magnitude of the vector V' , while the third case shows the combined effects of both. Although the effects of these parameters cannot be considered to be wholly independent, it is believed that the first-order effects were clearly indicated since the summation of the loads computed for cases (1) and (2) was nearly identical to those computed for case (3).

The study included four configurations,³ one nacelle and

³ The configurations selected were believed to be representative of current design trends. A four-bladed, right-hand propeller (described in ref. 4) was assumed to be installed on each configuration.

three wing-fuselage-nacelle combinations, which are shown in figure 7. The flow fields at the propeller plane were surveyed by use of a rake of directional pitot-static tubes.

The 1-P components of the calculated oscillating aerodynamic thrust load variations at the 0.7-radial station of the propeller, and the associated flow-field parameters are shown in figure 8. It can be seen that the variation of ψ , the direction of V' , produced a 1-P component, $(1-P)_\psi$, which was always phased such that it peaked at angular positions of approximately 90° and 270° , while the variation of θ and V_i/V_∞ , the magnitude of V' , also produced a significant 1-P component $(1-P)_\theta$, v_i/v_∞ the phase of which varied for different configurations. Further, since the total 1-P component, $(1-P)_T$, is the summation of these two components as expressed above, the phase and amplitude of the total 1-P component curve are directly dependent upon the amplitude ratio and phase relation of the two components due to ψ , and to θ and V_i/V_∞ . For the configurations investigated, $(1-P)_\psi$ was predominant in amplitude, its amplitude being never less than 87 percent of the total 1-P amplitude. Although for some configurations $(1-P)_\theta$, v_i/v_∞ had significant amplitude, it was phased such that its addition to $(1-P)_\psi$ caused the amplitude of $(1-P)_T$ to be only slightly larger than that of $(1-P)_\psi$. For other configurations, phasing of $(1-P)_\theta$, v_i/v_∞ was such that it could have increased the amplitude of $(1-P)_T$ over that of $(1-P)_\psi$. However its amplitude relative to that of $(1-P)_\psi$ was too small to be of significance. Insofar as the configurations investigated are typical of current design trends, it would seem that the amplitude of $(1-P)_\psi$ would be a good approximation of the amplitude of $(1-P)_T$, the value necessary for computing the 1-P stresses. It also is noted that $(1-P)_\psi$ always peaked at or very near the 90° and 270° angular positions and that at these positions, θ and V_i/V_∞ were generally 0° and 1.0, respectively.

DEVELOPMENT OF A SIMPLIFIED PROCEDURE FOR DETERMINING THE AMPLITUDE OF THE 1-P AERODYNAMIC THRUST LOAD

During the course of these studies, an important fact was discovered concerning the components of the oscillating aerodynamic load. For the cases investigated, no significant odd-order components above the fundamental, 1-P, were present. This fact makes possible the extraction of the 1-P component from the total variation by a simple operation which is independent of the number or amplitude of even-order components present. This simplicity stems from the fact that even-order harmonics repeat their magnitude and sense at half-cycle intervals of the fundamental, while odd-order components repeat their magnitude but are of opposite sense. If odd-order components above the fundamental are not present, one-half the arithmetic difference between values of the oscillating thrust load at any two angular positions 180° apart yields the exact magnitude of the 1-P component at those positions. Thus, computations at several angular positions around the propeller disk will define the exact variation of the 1-P component.

The amplitude and phase relation of the 1-P component can be determined by applying the method described at any four equally spaced angular positions. This is possible because (1) the variation of the oscillating aerodynamic

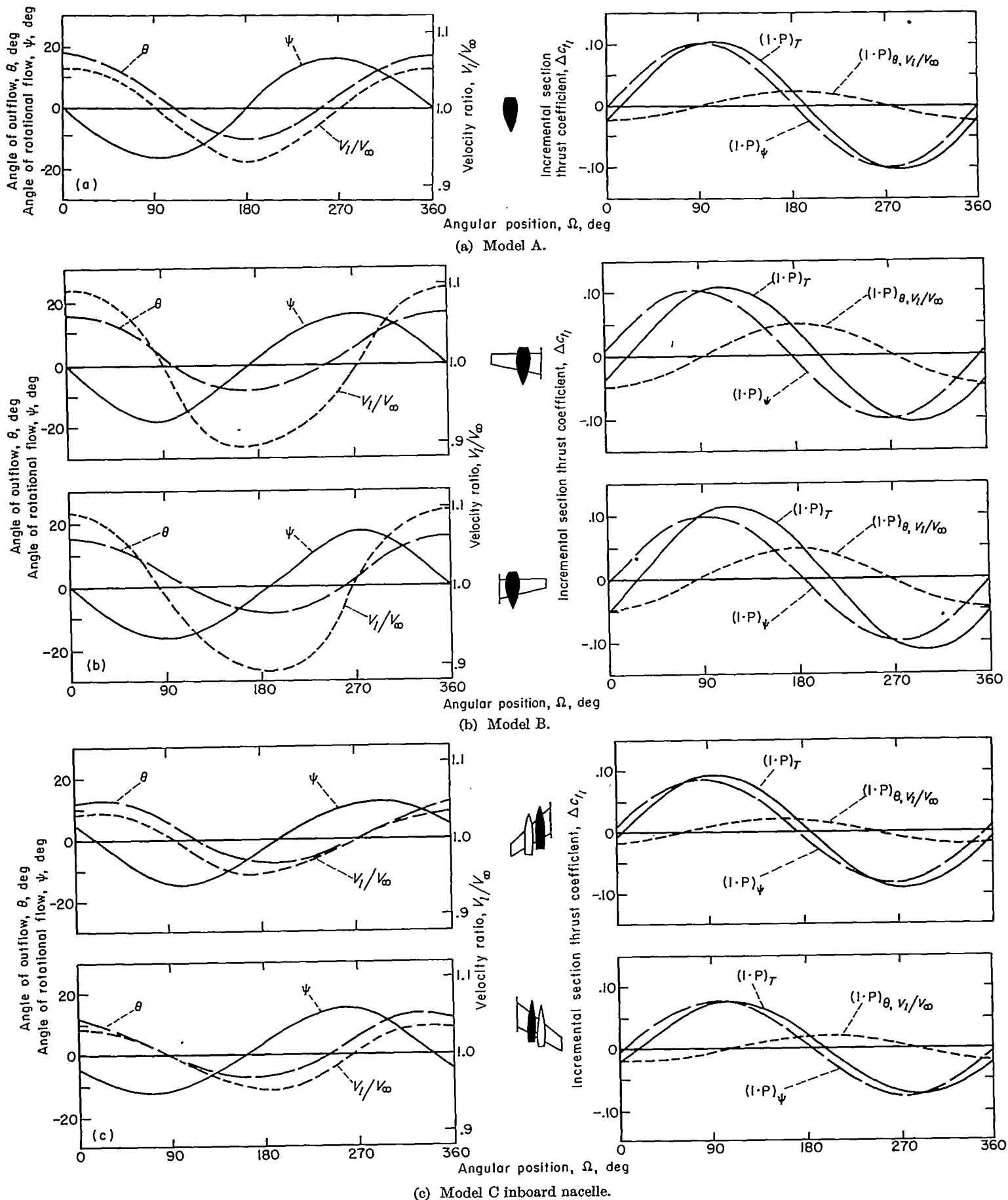


FIGURE 8.—The flow-field parameters and their effects on the $1-P$ variation of incremental section thrust coefficient for an isolated nacelle and several wing-fuselage-nacelle combinations.

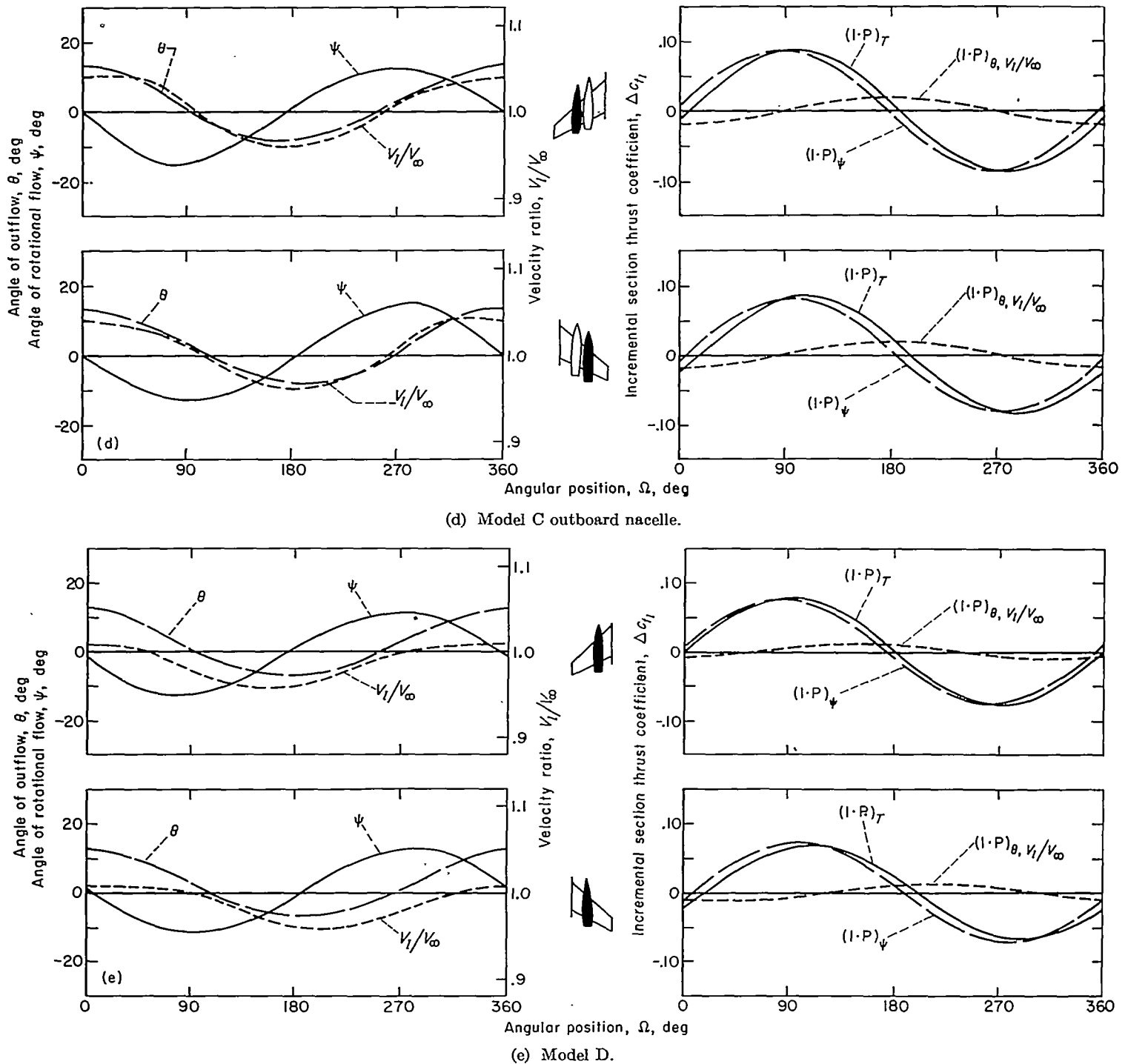


FIGURE 8.—Concluded.

load was periodic, (2) the components were all integer functions of one propeller revolution, and (3) no odd-order components above the fundamental were present. For example, at the specific angular positions $\Omega=0^\circ, 90^\circ, 180^\circ,$ and $270^\circ,$ expressions for determining the phase and amplitude of the $1\cdot P$ component are

$$\frac{1}{2} [(c_{t1})_{\Omega=90^\circ} - (c_{t1})_{\Omega=270^\circ}] = \delta c_{t1} \cos \varphi_a \quad (1a)$$

$$\frac{1}{2} [(c_{t1})_{\Omega=0^\circ} - (c_{t1})_{\Omega=180^\circ}] = \delta c_{t1} \sin \varphi_a \quad (1b)$$

where φ_a is the phase angle between the position at which the maximum magnitude of the $1\cdot P$ component occurs and the $\Omega=90^\circ$ position. As noted previously, for the cases investigated, values of φ_a were found to be quite small. Hence, it is believed plausible to make the approximation that

$$\delta c_{t1} \cos \varphi_a \approx \delta c_{t1} \quad (2)$$

A simplified procedure for determining the amplitude of the $1\cdot P$ aerodynamic thrust load is now evident which requires only the solution of equation (1a) with the foregoing approximation.

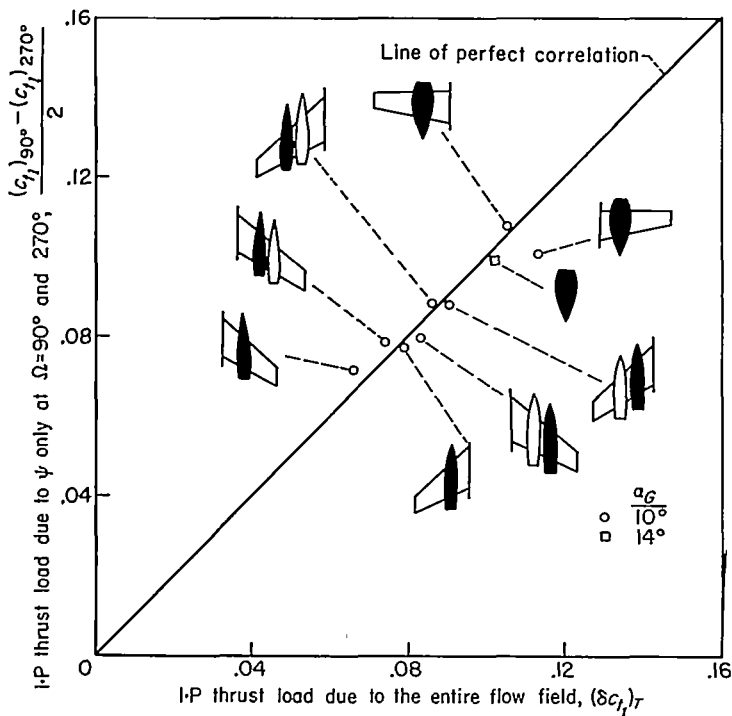
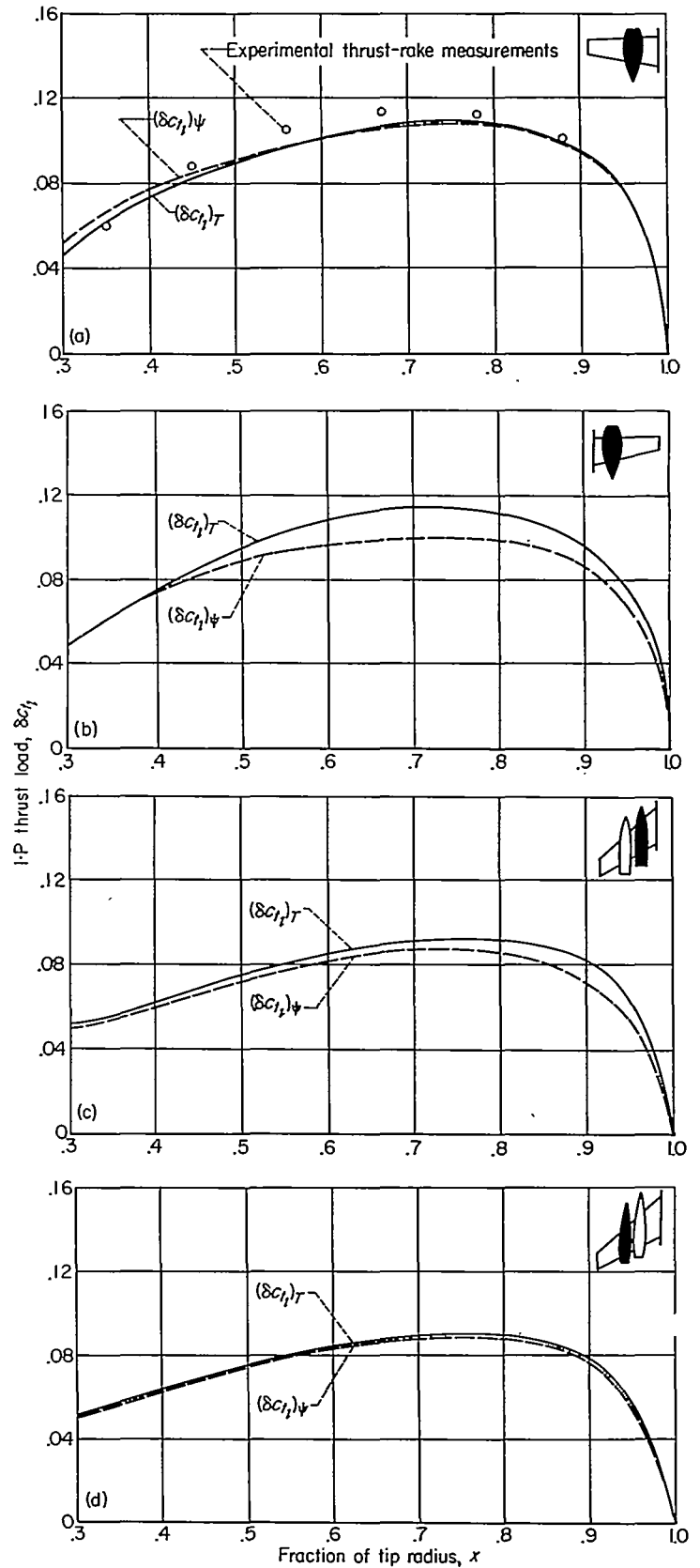


FIGURE 9.—Comparison of 1-P thrust loads as computed by the procedure of this report with those computed using the entire measured flow field for an isolated nacelle and several wing-fuselage-nacelle combinations; $\alpha=0.7$, $V_\infty=165$ mph, $n_p=1250$ rpm, $\beta_{0.75}=21.7^\circ$.

The introduction of this simplified procedure reduces the flow field information required to the values of the parameters at the $\Omega=90^\circ$ and 270° positions (the horizontal center line of the propeller disk). This fact and certain characteristics of the flow-field parameters preclude the need for experimental surveys of the flow field. It can be seen in figure 8 that, generally speaking, at the $\Omega=90^\circ$ and 270° positions θ and V_i/V_∞ are near the free-stream values of 0° and 1.0, respectively, as noted previously, while ψ is at nearly its maximum and minimum values. Hence, θ and V_i/V_∞ can be approximated by the free-stream values. Values of ψ on the horizontal center line of the propeller disk may be computed by the methods which are presented and evaluated in Appendixes B, C, and D. Thus, the need for experimental surveys of the flow field has been obviated.

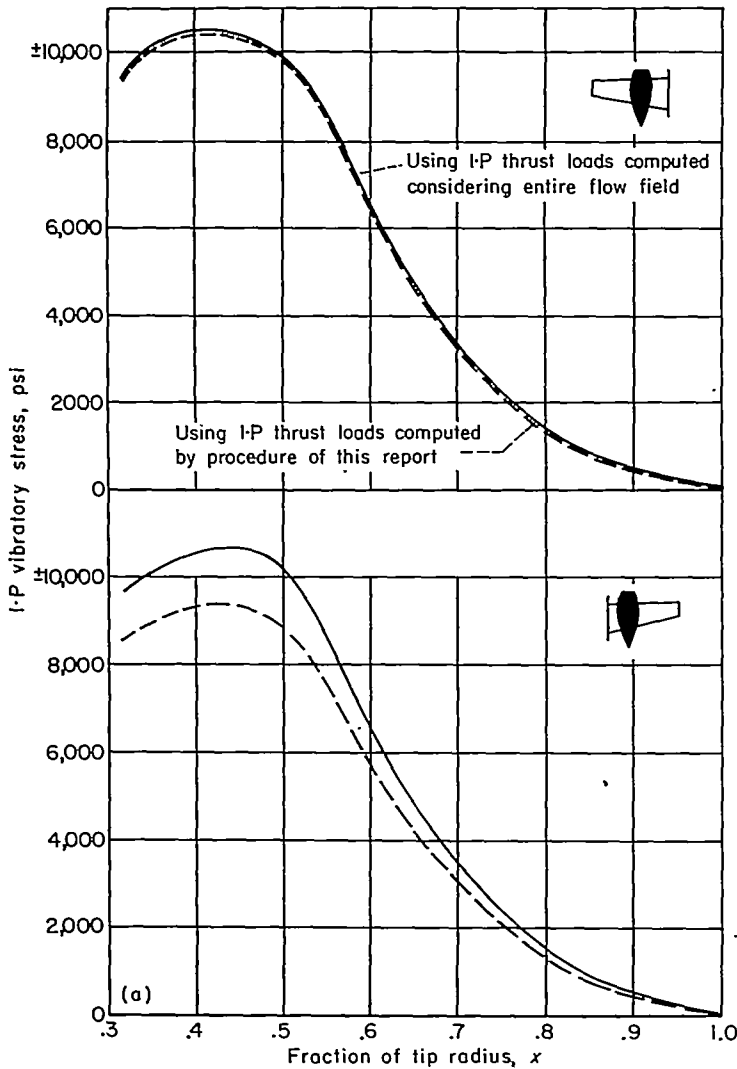
To indicate the accuracy and general applicability of the procedure, 1-P thrust loads on a propeller computed by the procedure are compared in figure 9 with those presented in figure 8 which were computed by 16-point computations based on all measured flow parameters. As noted above, the values of 0° and 1.0 were assumed for θ and V_i/V_∞ when applying the simplified procedure. Comparisons in figure 9 are at the 0.7-radial station of the propeller blade for all the test configurations. Comparisons of radial variations for two of the models are shown in figure 10 and, as further evaluation, the 1-P blade stresses computed using these load variations are compared in figure 11. From these figures, it is seen that the simplified procedure yielded generally satisfactory results for these configurations.⁴

⁴ A convenient design factor, now in common use, for indicating the relative stress levels on propellers for various flight conditions is the 1-P load exiting parameter Aq (refs. 1 and 2). By definition, A is identical to the absolute values of ψ at the horizontal center line of the Propeller disk.

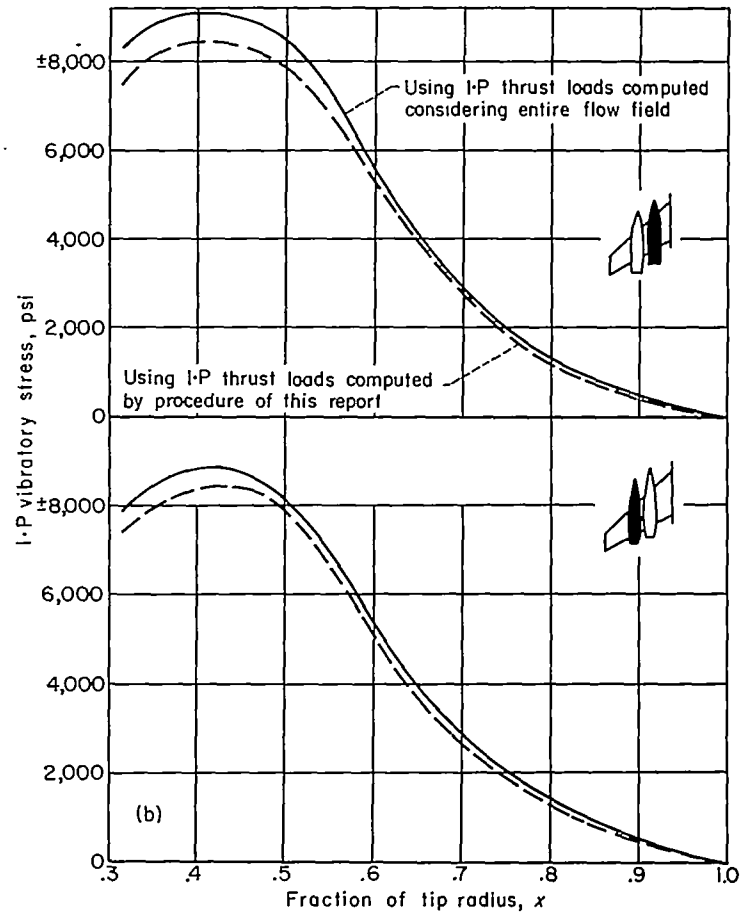


- (a) Model B port propeller.
- (b) Model B starboard propeller.
- (c) Model C port inboard propeller.
- (d) Model C port outboard propeller.

FIGURE 10.—Comparison of the radial variation of the 1-P thrust load computed by the procedure of this report with that computed using the entire measured flow field; $V_\infty=165$ mph, $n_p=1250$ rpm, $\beta_{0.75}=21.7^\circ$, $\alpha_G=10^\circ$.



(a) Model B.



(b) Model C.

FIGURE 11.—Comparison of 1-P vibratory stresses resulting from 1-P thrust loads computed by the procedure of this report with those resulting from 1-P thrust loads computed using the entire measured flow field; $V_\infty=165$ mph, $n_p=1250$ rpm, $\beta_{0.70}=21.7^\circ$, $\alpha_0=10^\circ$.

Evaluations of the methods for computing the values of ψ at the horizontal center line of the propeller disk are presented in the appendixes.

CONCLUDING REMARKS

The simplified procedure presented herein enables the rapid calculation of the 1-P thrust loads on propellers of tractor airplanes in pitch at zero yaw, without the need for tedious experimental surveys of the flow field at the propeller plane. The simplifications of the procedure have reduced the necessary flow-field information to a minimum; namely, the upflow angles at the horizontal center line of the propeller disk. These angles may be obtained simply by

the theoretical methods which are presented. Thereby, the need for experimental survey of the flow field is eliminated.

The evaluations of the simplified procedure which are shown indicate that the 1-P thrust loads computed for the airplane configurations investigated are generally satisfactory. These configurations are believed to be typical of current designs and it is believed that equal accuracy could be expected for configurations generally similar to those investigated.

AMES AERONAUTICAL LABORATORY
 NATIONAL ADVISORY COMMITTEE FOR AERONAUTICS
 MOFFETT FIELD, CALIF., Mar. 21, 1955

APPENDIX A

COMPUTATION OF BLADE-SECTION THRUST AND BLADE-SECTION NORMAL FORCE

The $1\text{-}P$ stress problem is primarily due to flatwise bending of the propeller blade resulting from $1\text{-}P$ oscillations in the blade normal force as the propeller turns through one revolution. The blade normal force at any angular and radial position is the sum of the components of the aerodynamic loads (i. e., the thrust and torque forces) perpendicular to the chord line of the blade element.

For the purposes of this investigation, it was desirable to express the normal force in as simple terms as possible. The normal force on a blade element, N_b , may be expressed as

$$N_b = t \cos \beta_x + f_q \sin \beta_x \quad (\text{A1})$$

where

t section thrust force

f_q section torque force

Equation (A1) may be rewritten in coefficient form and both the section thrust and the section torque may be expressed in terms of the section thrust due to blade lift only, c_{t_l} .

$$c_{N_b} = c_{t_l} \left(1 - \frac{\tan \gamma}{\cot \varphi}\right) \cos \beta_x + c_{t_l} \left(1 - \frac{\tan \gamma}{\cot \varphi}\right) \tan(\varphi + \gamma) \sin \beta_x \quad (\text{A2})$$

where $\tan \gamma = \frac{\text{blade-section drag}}{\text{blade-section lift}}$

Equation (A2) can be rearranged as follows

$$c_{N_b} = \frac{c_{t_l}}{\cos \beta_x} \left\{ \frac{\cos[(\gamma - \varphi) - 2(\beta_x - \varphi)] + \cos(\gamma + \varphi)}{\cos(\gamma - \varphi) + \cos(\gamma + \varphi)} \right\} \quad (\text{A3})$$

When conventional propellers are operated at low forward velocities (i. e., conditions corresponding to take-off and early climb where high $1\text{-}P$ excitations are encountered), the blade sections have high values of lift to drag ratio; hence γ is quite small as is the angle of attack of the blade section which is equal to the quantity $(\beta_x - \varphi)$. It can be seen that if these terms are neglected in the above expression, the term in the bracket becomes unity which is tantamount to saying that the drag force on a blade element contributes little to the blade element normal force. It is cautioned that such approximation may not be valid for all possible operating conditions. For simplicity, this assumption regarding the normal force was made for the work of this report and the normal force was expressed by the approximate relation

$$c_{N_b} = \frac{c_{t_l}}{\cos \beta_x} \quad (\text{A4})$$

Steady-state theories, applied in strip analysis form, have been developed to compute the aerodynamic loads on propellers operating in symmetrical flow fields where all the inflow is perpendicular to the propeller plane (e. g., see

ref. 11). It appeared reasonable that application of this type of analysis in stepwise computations might enable satisfactory computations of the values of c_{t_l} for propellers operating in distorted flow fields (thrust axis inclined or noninclined). The blade-element loads depend upon the angle of attack and velocity which the element experiences. The velocity involved is that in the plane tangent to the blade section path of rotation, V_B in figure 12. For a rotating blade element, the magnitude of V_B is defined by the inflow velocity V' and the rotational velocity $\pi n_r D x$. If the interference effects of the blades on each other are ignored, the angle of attack of the blade element is the blade geometric setting β_x minus the helix angle φ_o .

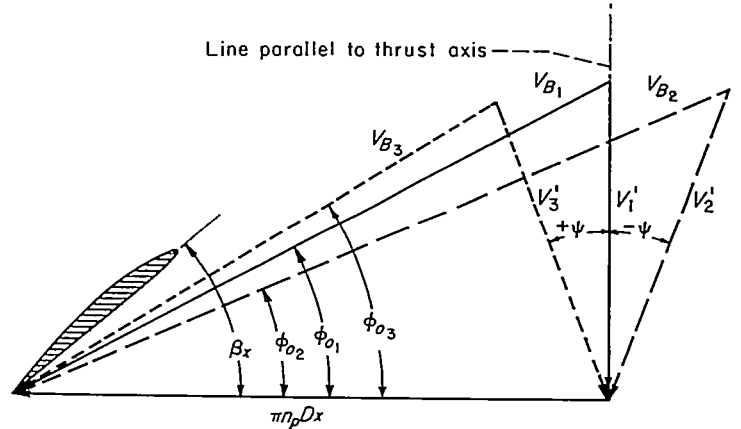


FIGURE 12.—Velocity diagram of propeller blade section.

The distorted flow-field case differs from the symmetrical case in that V' is not always perpendicular to the propeller plane nor of constant magnitude, but varies in direction and magnitude with angular position Ω of the blade. In figure 12, subscript 1 represents the symmetrical case while subscripts 2 and 3 represent the extremes of the variation for the distorted case. Consequently, it is apparent that these variations must be taken into account in the computations.

The equation for the coefficient of thrust on a blade element for a propeller in a symmetrical flow field including blade interference effects is

$$c_t = \kappa \pi^2 x^3 \frac{\alpha_t}{57.3} \frac{(\cot \varphi - \tan \gamma)}{\left(\cot \varphi + \frac{\alpha_t}{57.3}\right)^2} \quad (\text{A5})$$

where

- φ $\varphi_o + \alpha_t$
- φ_o $\tan^{-1}(V_\infty / \pi n_r D x)$
- α_t propeller-induced angle of inflow, deg
- κ Goldstein correction factor for a finite number of blades
- γ $\tan^{-1}\left(\frac{\text{blade-section drag}}{\text{blade-section lift}}\right)$

For the distorted flow-field case, it is necessary to modify the equation to account for variations in both direction and magnitude of V' described above. Thus,

$$c_{i_t} = \kappa \pi^3 x^3 \frac{\alpha_t}{57.3} \frac{(\cot \varphi - \tan \gamma)}{\left(\cot \varphi + \frac{\alpha_t}{57.3}\right)^2} \left(1 - \frac{V' \sin \psi}{\pi n_p D x}\right)^2 \quad (A6)$$

for which it is important to note that

$$\varphi_o = \tan^{-1} \left(\frac{V' \cos \psi}{\pi n_p D x - V' \sin \psi} \right)$$

In determining α_t (the interference effects), the assumption is made that all the blades are operating at the same flow conditions as the blade being considered.

The expression for c_i may be simplified to consider only the section thrust due to blade lift, c_{i_p} , by ignoring the blade drag term, $\tan \gamma$. Thus

$$c_{i_t} = \kappa \pi^3 x^3 \frac{\alpha_t}{57.3} \frac{\cot \varphi}{\left(\cot \varphi + \frac{\alpha_t}{57.3}\right)^2} \left(1 - \frac{V' \sin \psi}{\pi n_p D x}\right)^2 \quad (A7)$$

This is the expression used in the studies to calculate the values of c_{i_t} using all measured values of the flow-field parameters. When the values of 0° and 1.0 are substituted for θ and V_i/V_∞ as in the simplified procedure of the report, V' becomes equal to V_∞ . Hence, V_∞ is substituted for V' in the last term of equation (A7) and in the expression for φ_o .

$$c_{i_t} = \kappa \pi^3 x^3 \frac{\alpha_t}{57.3} \frac{\cot \varphi}{\left(\cot \varphi + \frac{\alpha_t}{57.3}\right)^2} \left(1 - \frac{V_\infty \sin \psi}{\pi n_p D x}\right)^2 \quad (A8)$$

where

$$\varphi_o = \tan^{-1} \left(\frac{V_\infty \cos \psi}{\pi n_p D x - V_\infty \sin \psi} \right)$$

APPENDIX B

METHODS FOR DETERMINING THE VALUES OF ψ AT THE HORIZONTAL CENTER LINE OF A PROPELLER DISK

The value of ψ at the horizontal center line of a propeller disk is the summation of the geometric angle of attack of the thrust axis and the upwash angles induced by the various components of the airplane at the horizontal center line of the propeller disk, expressed as

$$\psi = \alpha_{\text{geometric}} + \epsilon_{\text{wing}} + \epsilon_{\text{adjacent bodies}} + \epsilon_{\text{body containing thrust axis}} \quad (B1)$$

To determine these angles theoretically, the total angle of attack of each component must be known so that its contribution to ψ can be computed. Each component total angle of attack, like ψ , is the result of a geometric angle of attack plus an induced angle resulting from the upwash of other components. It is clear that to obtain an exact total angle of attack for each component, an iterative process would be required. However, within engineering accuracy, it was found possible to avoid this process.

In the case of the wing, it was found that ϵ_{wing} could be adequately predicted by considering only an isolated wing at the geometric angle of attack; that is, the adjacent bodies influenced the wing total angle of attack so slightly that the resultant change in ϵ_{wing} was negligible.

This conclusion is verified in figure 13 where ϵ_{wing} computed by the method presented in Appendix C from measured span loading on a wing affected by a nacelle is compared to that computed for the isolated wing. The differences are seen to be negligible.

In the case of determining the correct total angle of attack for a body, it was found that the effect of upwash from the wing and from other bodies generally could not be ignored. The wing upwash contribution to the angle of attack of a body can be computed by considering only the wing geometric angle of attack, since bodies have been shown to have little effect on the wing induced upwash. For a wing-body combination (i. e., a fuselage or single-engine airplane) the body effective angle of attack is taken as the arithmetic sum of the geometric angle of attack of the body and the

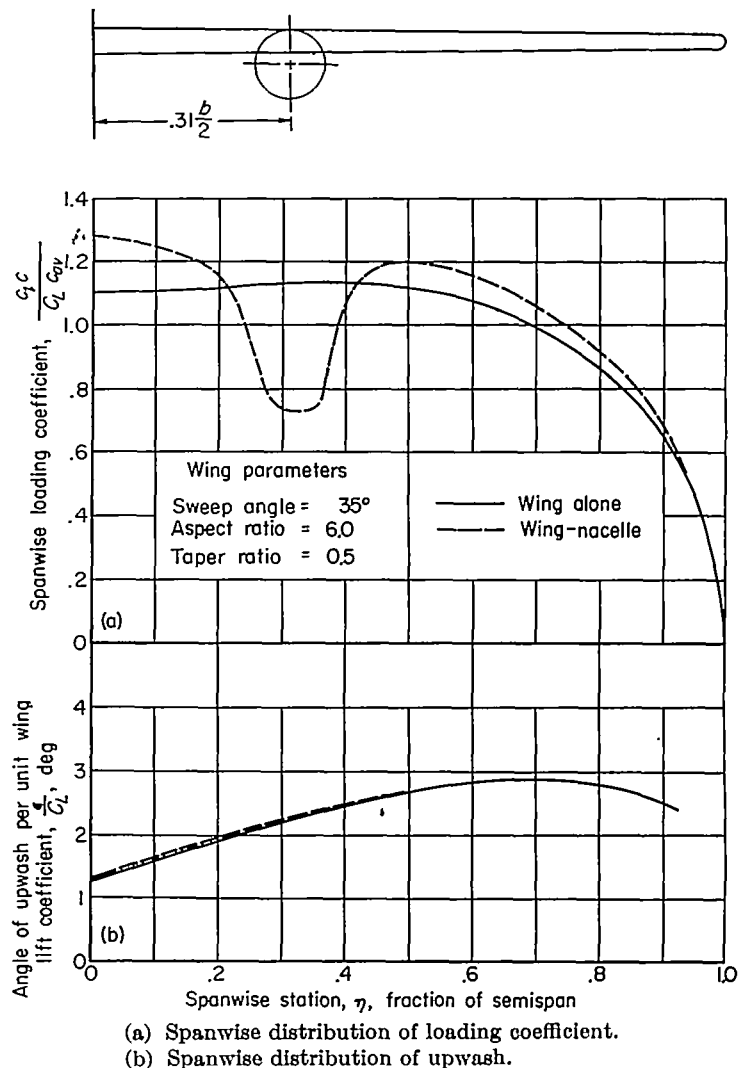


FIGURE 13.—Comparison of measured spanwise load distribution for an isolated wing and a wing-nacelle combination, and the resultant computed upwash distribution at a distance of one chord ahead of the wing leading edge; $M=0.18$, $C_L=0.32$.

value of wing upwash in the propeller plane at the axis of the body

$$\alpha_{eff} = \alpha_{geometric} + \epsilon_{wing} \tag{B2}$$

For the case of a configuration having more than one body (i. e., multiengine-type airplanes where the propulsive units are housed in nacelles outboard of a fuselage) the total angle of attack of a second body, for illustration assumed to be a nacelle, is expressed as

$$\alpha_{eff_n} = \alpha_{geometric} + \epsilon_{wing} + \epsilon_{adjacent\ body} \tag{B3}$$

where the value of ϵ_{wing} is the magnitude of wing upwash in the propeller plane at the nacelle axis. The value of $\epsilon_{adjacent\ body}$ at the nacelle axis is computed for the adjacent body at the effective angle of attack determined from equation (B2). This ignores the fact that the adjacent body is under the influence of the nacelle; this second-order effect is believed to be negligible.

While wing upwash is always important, the importance of considering upwash from adjacent bodies when obtaining a body total angle of attack varies widely depending on body proximity, relative size, and longitudinal position. For example, in the case of a multiengine airplane, the effect of one nacelle on the total angle of attack of the other can be shown to be small if the first nacelle lies behind the propeller plane of the second. Thus wing sweep would vary the importance of upwash from adjacent nacelles in finding the total angle of attack of a given nacelle. On the other hand, if the adjacent body were large compared to a nacelle, for example, a fuselage where the fuselage nose was downstream of the propeller plane, its effect on the nacelle total angle of attack would be important. Generally speaking, any body which extends ahead of the propeller plane at which ψ is being computed will have a significant effect on the total angle of attack of the body containing the thrust axis corresponding to that propeller plane; for example, usually fuselages and inboard nacelles both must be taken into account in finding the total angle of attack of the outboard nacelle in four-engine swept-wing configurations, whereas only the fuselage significantly affects the inboard nacelle.

To evaluate the use of equation (B1) and the methods which have been described, the variations of the upwash angle due to the various components and the curve representing the summation of these and the geometric angle of attack of the thrust axis are shown in figure 14 for several wing-nacelle-fuselage combinations at a Mach number of 0.22. Also shown is a comparison of these results with the measured values which indicates good agreement. Similar

comparisons are made in figure 15 for the wing-nacelle-fuselage combination described in reference 9 for a Mach number range from 0.25 to 0.92. In computing the upwash for this combination, account was taken of compressibility effects, except for the effects on the body-induced upwash, whose mechanics were not clearly understood. Good agreement between computed and measured upwash angles is indicated up to a Mach number of about 0.8. Compressibility effects are discussed more fully in Appendixes C and D.

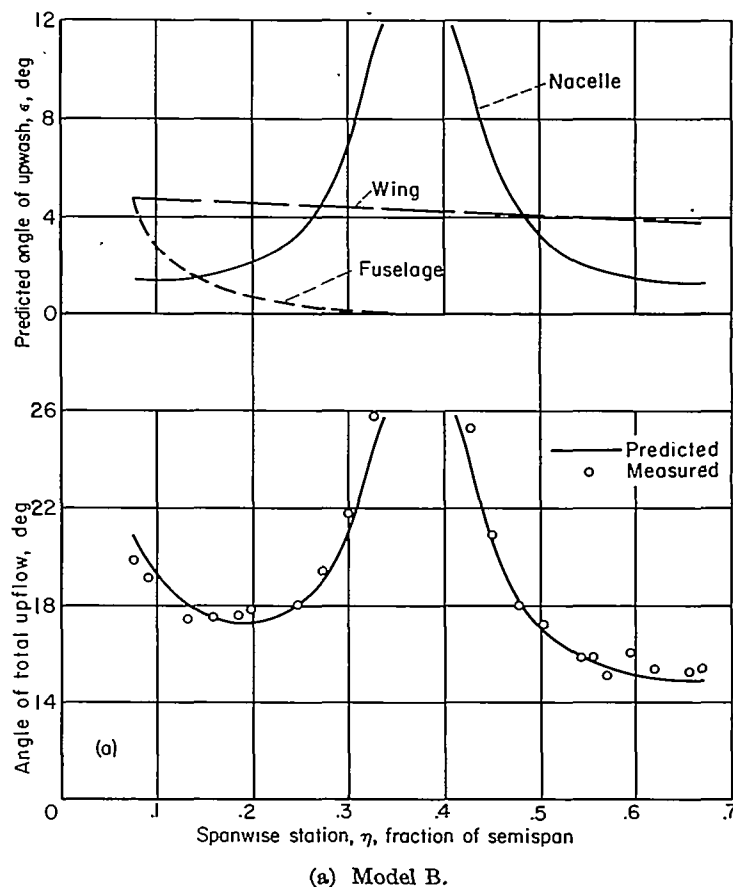
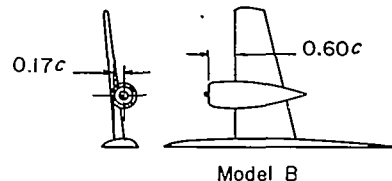


FIGURE 14.—Measured and predicted upflow angles and predicted upwash components at the horizontal center line of the propeller disks of several wing-fuselage-nacelle combinations; $\alpha_0 = 10^\circ$. $M = 0.22$.

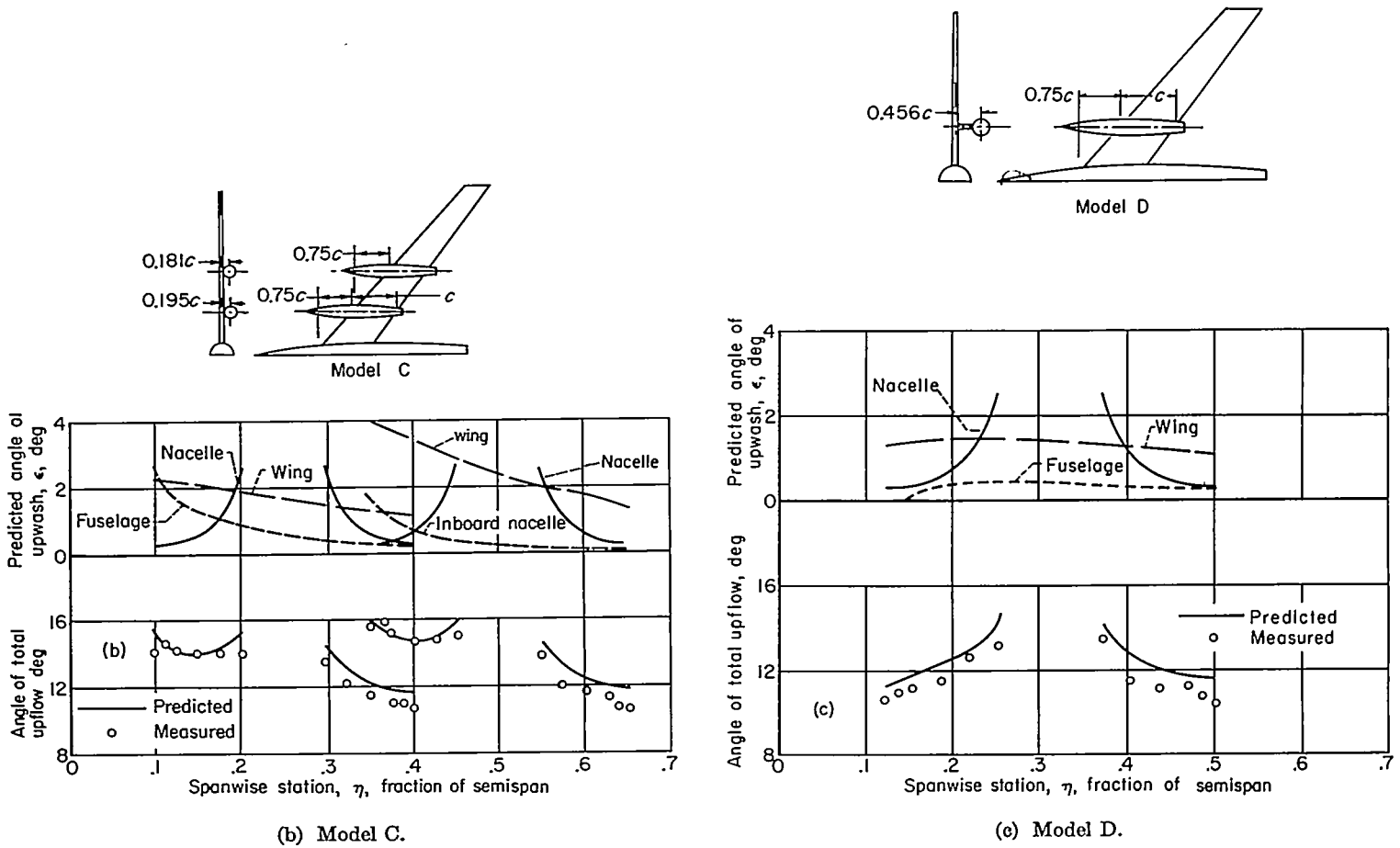


FIGURE 14.—Concluded.

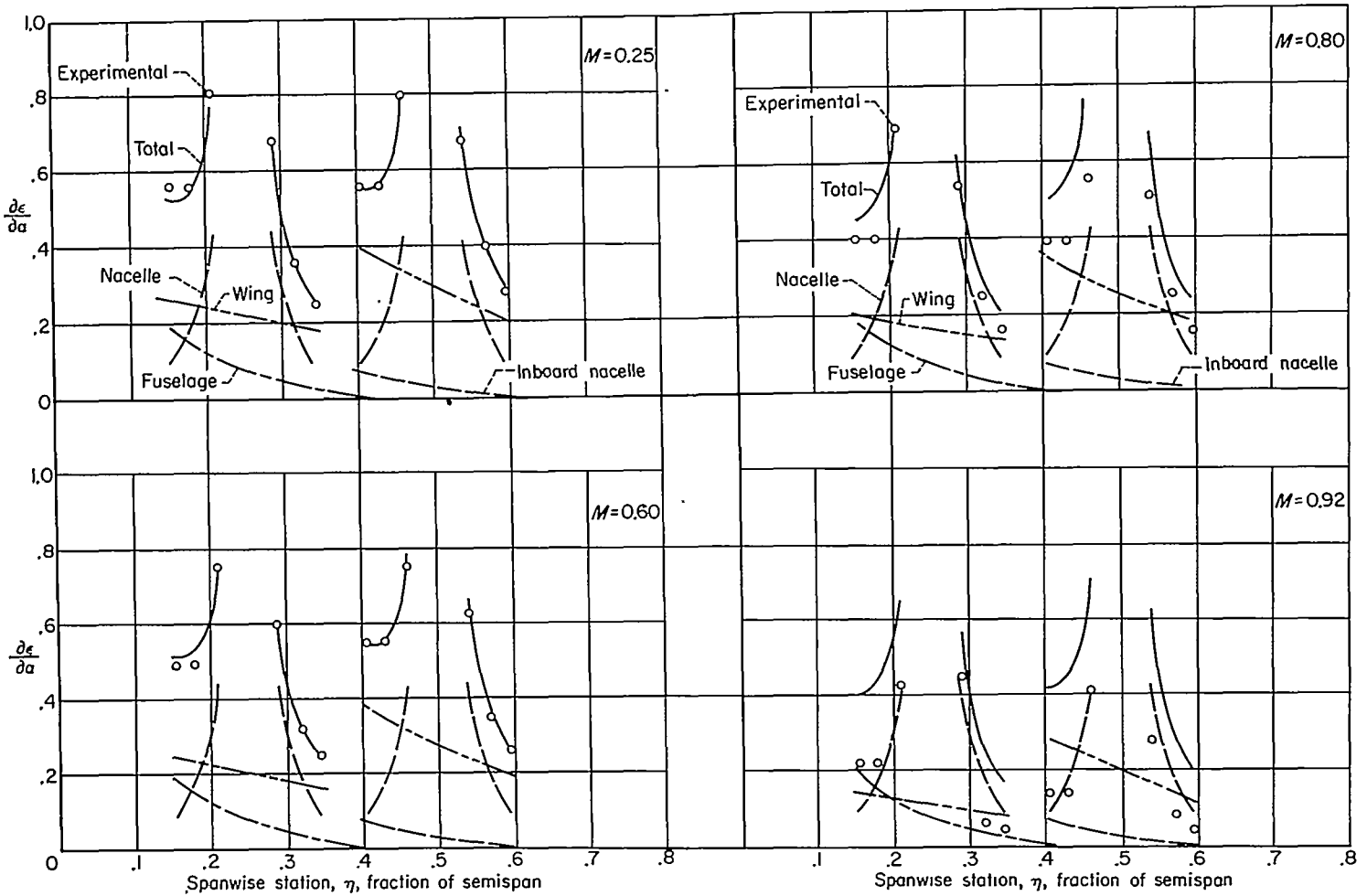
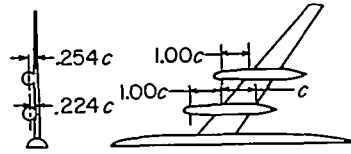


FIGURE 15.—The effects of Mach number on the upwash at the horizontal center line of the propeller disks of a wing-fuselage-nacelle combination utilizing a swept wing.

APPENDIX C

A METHOD FOR COMPUTING THE WING-INDUCED UPWASH ANGLES AT THE HORIZONTAL CENTER LINE OF A PROPELLER DISK

PREDICTION OF THE UPWASH ANGLE INDUCED IN THE EXTENDED WING-CHORD PLANE BY WINGS OF ARBITRARY PLAN FORM

It was shown in reference 12 that for a known symmetrical load distribution on a wing, the wing-induced downwash could be computed by use of influence coefficients designated a_{rn} coefficients which were presented therein. The same basic equations derived for the downwash computations are applicable for upwash computations, but new values of the a_{rn} coefficients are required.

The upwash can be found at specific points in the extended chord plane between the wing tips and ahead of the wing leading edge. The general expression for the upwash is given as

$$\left(\frac{w}{V_\infty}\right)_{z, y, r} = \sum_{n=1}^4 a_{rn} G_n \tag{C1}$$

where

- G_n dimensionless circulation $\frac{\Gamma}{bV_\infty}$ identical to the load coefficient $\frac{c_l c}{2b}$ at span station n
- M free-stream Mach number
- b span of a wing measured perpendicular to the vertical plane of symmetry, ft
- c local chord of a wing measured in a plane parallel to the vertical plane of symmetry, ft

- c_l section lift coefficient of a wing, $\frac{\text{section lift}}{q_\infty c}$
- n an integer defining a spanwise station on the wing quarter-chord line for which the value of circulation is defined
- q_∞ free-stream dynamic pressure, lb/sq ft
- w induced velocity, perpendicular to the mean chord line of the wing, positive for upwash, ft/sec
- x_w longitudinal distance from the wing quarter-chord line, ft
- β compressibility factor, $\sqrt{1-M^2}$
- ν an integer defining a specific point within the wing plan form for which the boundary condition of no flow through the wing is applied
- τ longitudinal coordinate $\frac{x_w}{b/2}$, semispans

The $a_{\nu n}$ coefficients are obtained from figure 16. The specific stations at which the upwash may be found correspond to $\nu=1, 2, 3, 4$ or $\eta_r = \cos(\nu\pi/8) = 0.924, 0.707, 0.383$ and 0, respectively. For convenience, the preceding equation is rewritten so that the upwash angle and loading distribution are in terms of unit lift coefficient. Thus

$$\left(\frac{w/V_\infty}{\beta C_L/K_{av}}\right)_{\tau/\beta, \eta} = \frac{1}{2} \left[\frac{\beta(b^2/S)}{K_{av}} \right] \sum_{n=1}^4 a_{\nu n} \left(\frac{c_l c}{C_L c_{av}}\right)_n \quad (C2)$$

where

$$\frac{\epsilon}{\beta C_L} = \frac{1}{4\pi\beta b^2/S} \left\{ - \left[\frac{1-\eta}{\zeta^2+(1-\eta)^2} \right] - \left[\frac{1+\eta}{\zeta^2+(1+\eta)^2} \right] + \right.$$

$$\frac{\left[\frac{\tau/\beta}{(\tau/\beta)^2 + \zeta^2/\cos^2 \Delta_\beta} \right] \left[\left(\tau/\beta \tan \Delta_\beta + \frac{1-\eta}{\cos^2 \Delta_\beta} \right) \right] + \left[\frac{1-\eta}{\zeta^2+(1-\eta)^2} \right] \left\{ \left[\tau/\beta + (1-\eta) \tan \Delta_\beta \right] \right\}}{\sqrt{[\tau/\beta + (1-\eta) \tan \Delta_\beta]^2 + (1-\eta)^2 + \zeta^2}}$$

$$\frac{\left[\frac{2\eta \tan \Delta_\beta - \tau/\beta}{(2\eta \tan \Delta_\beta - \tau/\beta)^2 + \zeta^2/\cos^2 \Delta_\beta} \right] \left[\left(\tau/\beta \tan \Delta_\beta + \frac{1-\eta}{\cos^2 \Delta_\beta} \right) + 2\eta \right] - \left[\frac{1+\eta}{\zeta^2+(1+\eta)^2} \right] \left\{ \left[\tau/\beta + (1-\eta) \tan \Delta_\beta \right] \right\}}{\sqrt{[\tau/\beta + (1-\eta) \tan \Delta_\beta]^2 + (1+\eta)^2 + \zeta^2}}$$

$$\left. \frac{\left[\frac{\tau/\beta}{(\tau/\beta)^2 + \zeta^2/\cos^2 \Delta_\beta} \right] \left(\tau/\beta \tan \Delta_\beta - \frac{\eta}{\cos^2 \Delta_\beta} \right) - \left[\frac{2\eta \tan \Delta_\beta - \tau/\beta}{(2\eta \tan \Delta_\beta - \tau/\beta)^2 + \zeta^2/\cos^2 \Delta_\beta} \right] \left[\left(\tau/\beta \tan \Delta_\beta - \frac{\eta}{\cos^2 \Delta_\beta} \right) + 2\eta \right]}{\sqrt{(\eta \tan \Delta_\beta - \tau/\beta)^2 + \eta^2 + \zeta^2}} \right\} \quad (C3)$$

where

- η lateral coordinate from the wing longitudinal center line, semispans
- ζ vertical coordinate from the wing chord plane, semispans

From the variation thus obtained, the upwash angle at any position above or below the extended chord plane may be expressed as a percentage of the value at the chord plane.

- $\frac{c_l c}{C_L c_{av}}$ span loading coefficient
- S wing area, sq ft
- c_{av} average chord of a wing, $\frac{S}{b}$, ft
- C_L lift coefficient of a wing, $\frac{\text{wing lift}}{q_\infty S}$
- K_{av} average of the ratios of the experimental section lift curve slope to the theoretical value $\frac{2\pi}{\beta}$, all at the same Mach number

Both $a_{\nu n}$ and $c_l c/C_L c_{av}$ are affected by compressibility, since they have been determined as functions of the parameters $\beta(b^2/S)/K_{av}$ and Δ_β .

MODIFICATION OF THE METHOD TO PREDICT UPWASH ANGLE AT POSITIONS ABOVE AND BELOW THE EXTENDED WING-CHORD PLANE

This modification is based on the assumption that the vertical variation of the wing-induced upwash angle is similar to that induced by a simple horseshoe vortex; that is, that a percentage ratio can be established between the two. For low Mach numbers, the bound portion of the horseshoe vortex has the same sweep as the wing quarter-chord line,¹ and lies in the wing chord plane. For a value of η and τ/β , the vertical variation of upwash angle due to a horseshoe vortex can be obtained from the following equation which corresponds to equation (34) of reference 13.

Based on the foregoing assumption, the value obtained on the extended wing-chord plane for a wing of arbitrary plan form may be multiplied by this percentage value to obtain the upwash angle induced by the wing at the same position above or below the chord plane. A typical example of the variations of the upwash angle expressed in percentage of the wing-chord plane value are shown in figure 17 for a horseshoe vortex swept back 40°.

¹ For high Mach numbers, the horseshoe vortex should have a sweep angle Δ_β given by $\tan \Delta_\beta = (\tan \Lambda)/\beta$ in accordance with the Prandtl-Glauert rule.

EFFECTS OF COMPRESSIBILITY ON THE WING-INDUCED UPWASH

The Prandtl-Glauert rule, which accounts for the effects of compressibility, is directly applicable to the subject method. The basis for the corrections applied to the method as simply stated in the Prandtl-Glauert rule is that as the Mach number is increased, the span load distribution of a wing distorts as though its longitudinal dimensions were increasing as the ratio $1/\beta$. Thus, the effects of Mach number on a given wing can readily be considered by finding the span loading at zero Mach number of a properly distorted wing.

Since the wing-induced upwash distribution is directly dependent upon the span loading, the effects of compressibility on this factor were investigated. A typical example of the compressibility effects on a span loading is shown in figure 18. The small differences which are shown have little significance in terms of the upwash induced in the extended wing-chord plane. Hence, the span load for zero Mach number can be used satisfactorily.

It can be seen that increasing the longitudinal dimensions of the wing results in increasing the angle of sweep and increasing each local chord while leaving the span and taper unaffected. Thus, the distance from the quarter-chord line to a given point in the chord plane must also be increased by the ratio $1/\beta$. The compressibility effects on the effective sweep angle are sizable. For example, increasing the Mach number from 0.33 to 0.90 changes the effective sweep angle of a 40° sweptback wing from $41\frac{1}{2}^\circ$ to $62\frac{1}{2}^\circ$. In terms of the wing-induced upwash, this effectively increases the distance from a point on the extended wing-chord plane to the vortex core and thereby reduces the core's influence at that point. Hence, the values of τ and Λ must be corrected to τ/β and Λ_β before entering the charts of the $a_{r,n}$ coefficients.

It is obvious that for a given value of τ/β , the compressibility effects are not constant for all sweep angles. To illustrate this point, typical examples of the upwash angle distribution, spanwise for constant values of τ/β , are shown for wings with 0° and 40° of sweep. Figure 19 shows there

is no variation of the upwash angle with Mach number for an unswept wing at a given τ/β since $\tan \Lambda$ is zero. However, for the wing swept back 40° , it is shown in figure 20 that an increase from a Mach number of 0.33 to 0.90 produced sizeable changes in the upwash angle distributions at a constant τ/β .

PROCEDURE FOR APPLYING THE METHOD TO OBTAIN THE WING-INDUCED UPWASH ANGLES AT THE HORIZONTAL CENTER LINE OF THE PROPELLER PLANE

The first step is to obtain the span load distribution (e. g., by the methods of ref. 12); Mach number effects on the span load need not be considered as shown previously. Second, determine the τ/β variation and the value of Λ_β at the particular Mach number for the propeller plane locations in the extended wing-chord plane. The maximum and minimum values of τ/β will define the range over which computations must be made. Next, compute the values of ϵ/C_L at the four control points on the span for constant values of τ/β over the range defined above. This is accomplished by substituting the values of the span load and the $a_{r,n}$ coefficients derived from the charts in equation (C2). If necessary, these values should then be modified for displacements above and below the chord plane by means of equation (C3). The fairing of the resulting data points will yield the spanwise distributions of ϵ/C_L for constant values of τ/β ; a plot similar to figure 20. Using the values of τ/β previously determined, the propeller plane can be located on this plot as shown in figure 20 and the values of ϵ/C_L determined at any radial station.

To illustrate the method and the results obtained, the variations of τ/β and ϵ/C_L across the horizontal center line of the propeller disks of two representative airplane configurations are shown in figures 21 and 22 for Mach numbers of 0.33 and 0.90. The geometric characteristics of the components of these configurations were identical except that one wing panel was unswept and the other was swept back 40° .

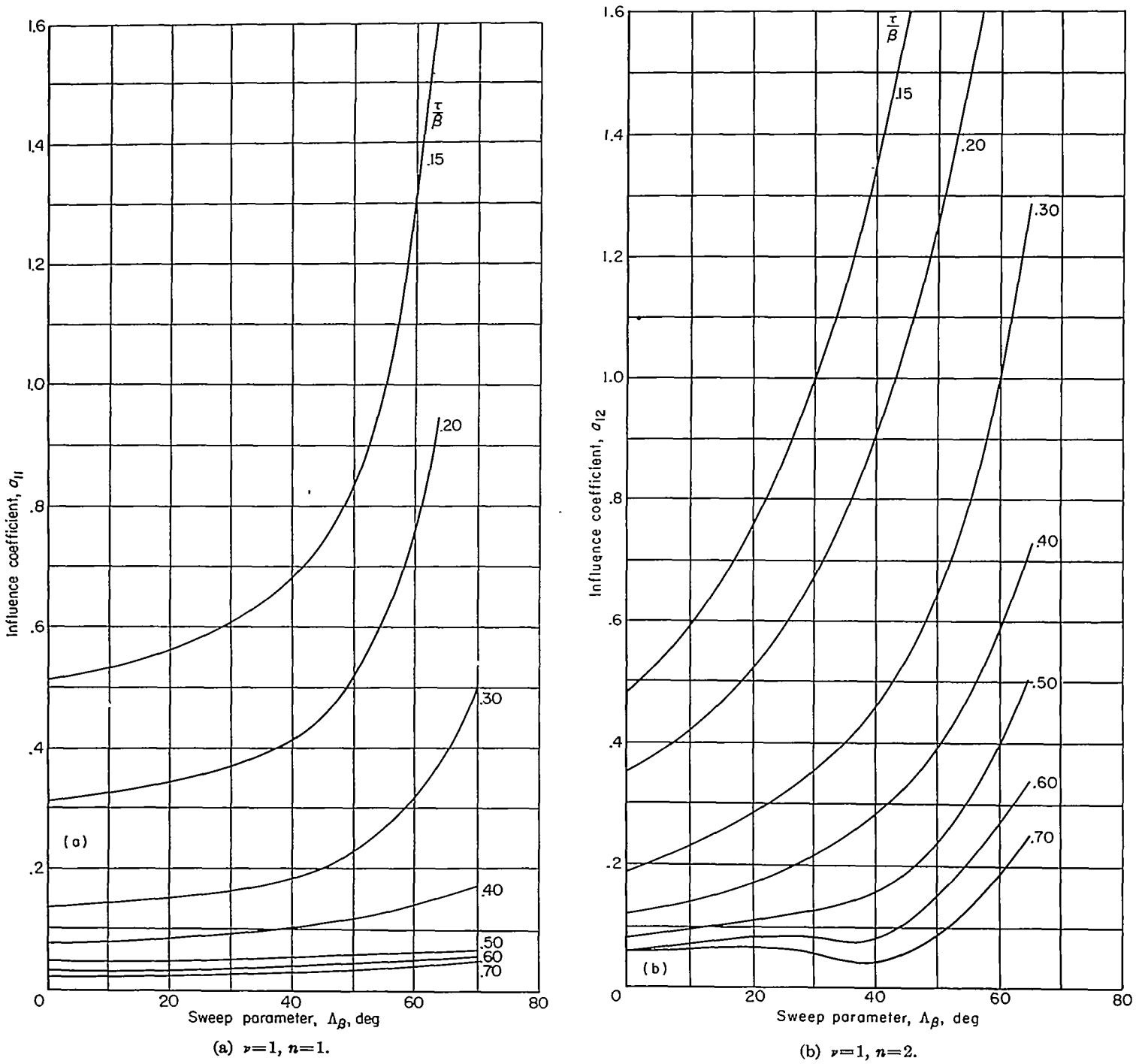


FIGURE 16.—Influence coefficients, $a_{r,n}$, for symmetric span loading plotted as a function of the sweep parameter, $\Delta\beta$, for various distances ahead of the wing quarter chord line, τ/β .

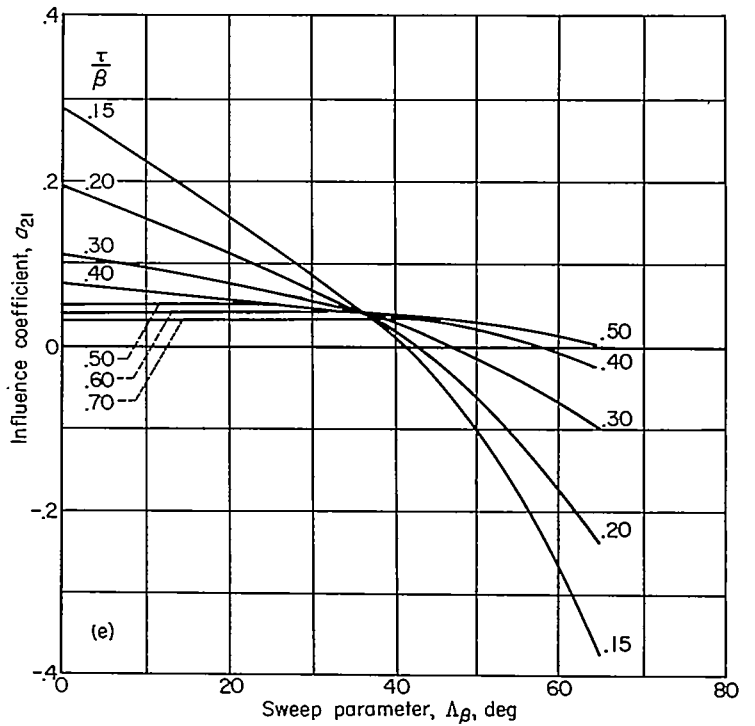
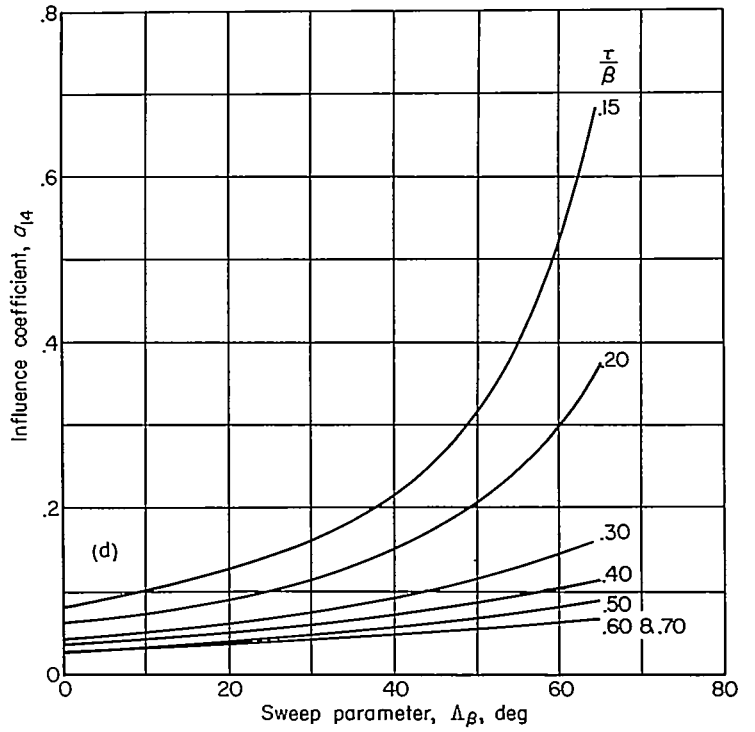
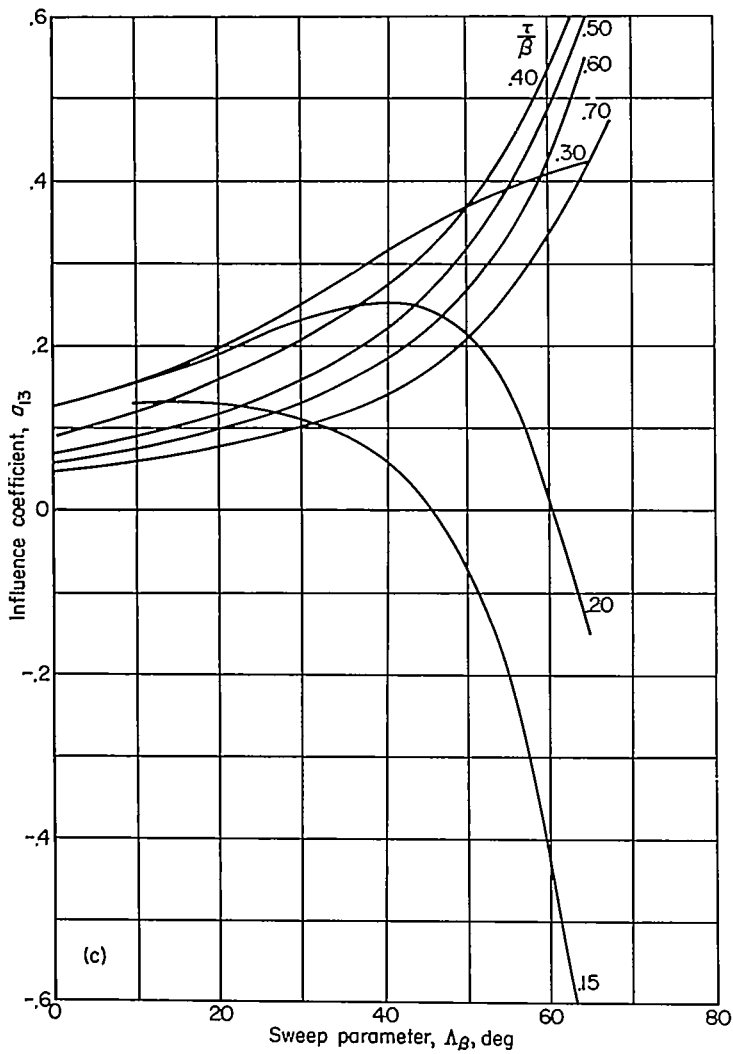


FIGURE 16.—Continued.

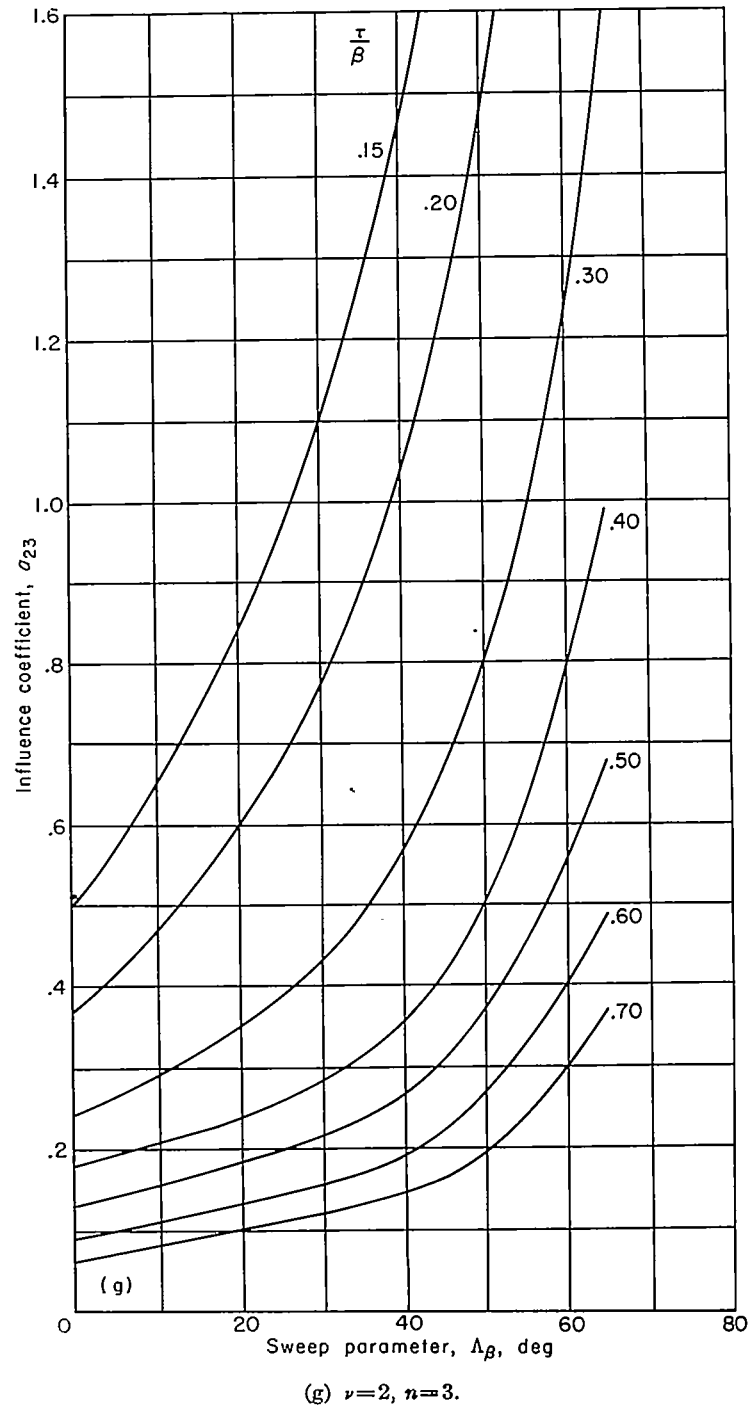
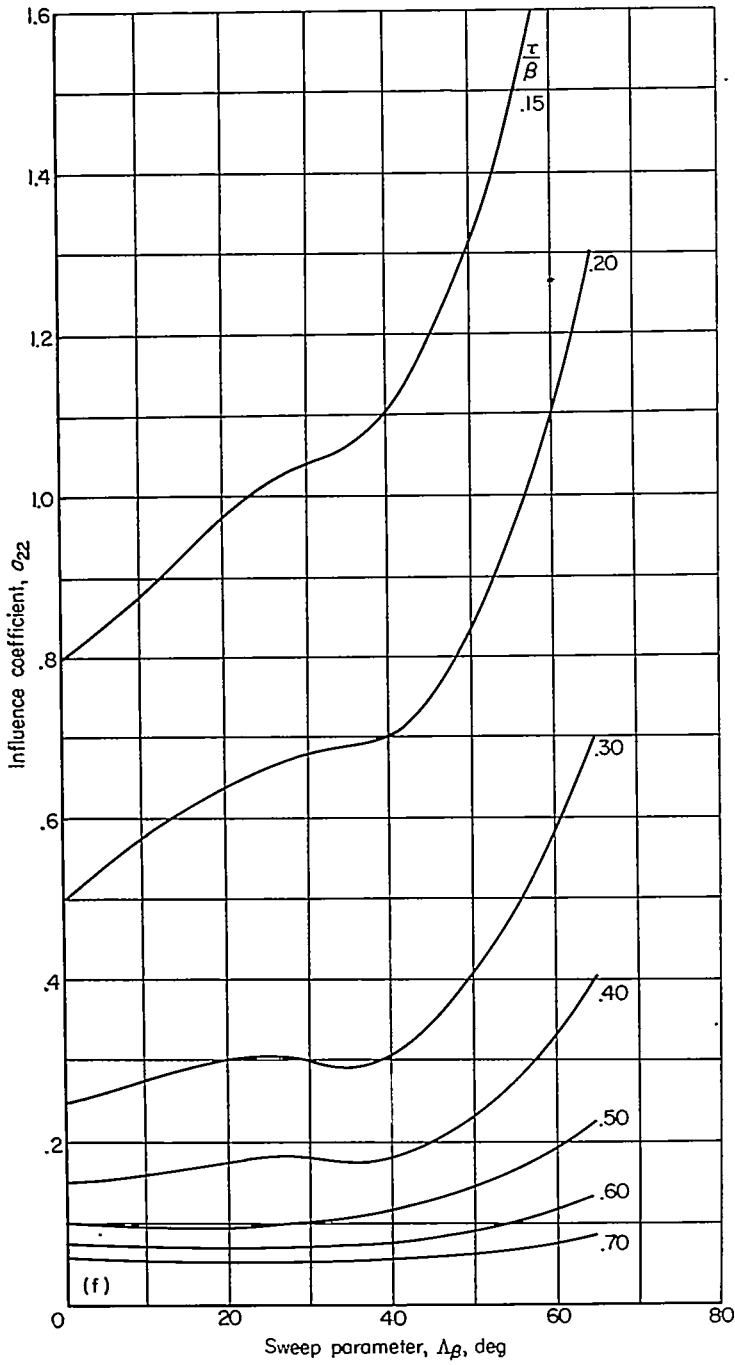


FIGURE 16.—Continued

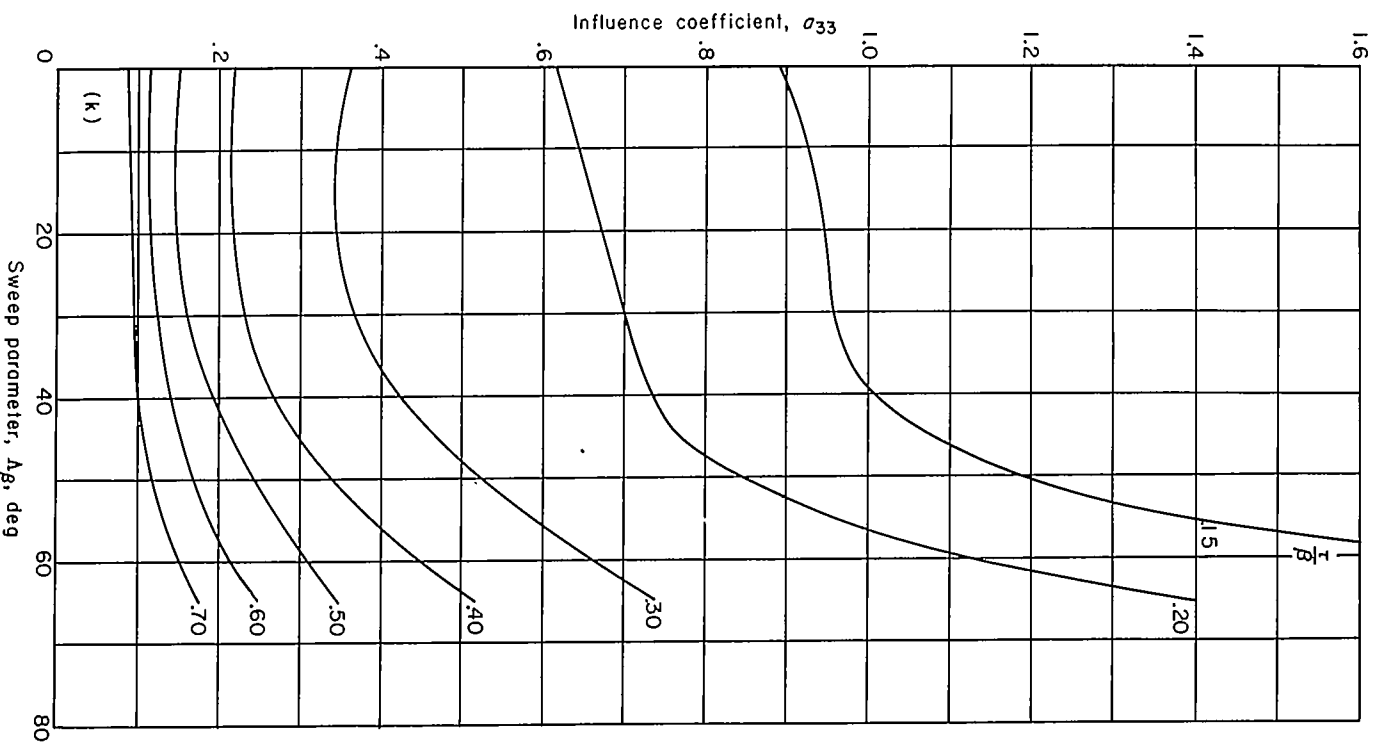
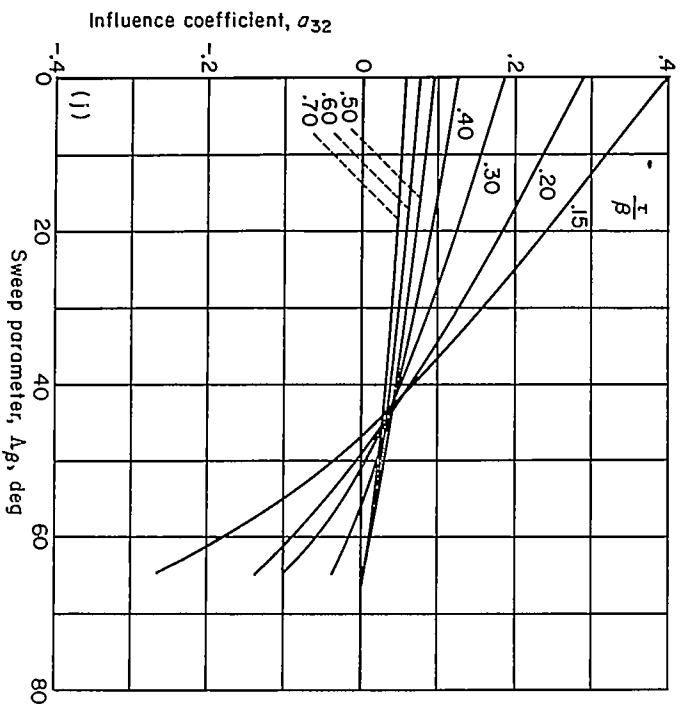
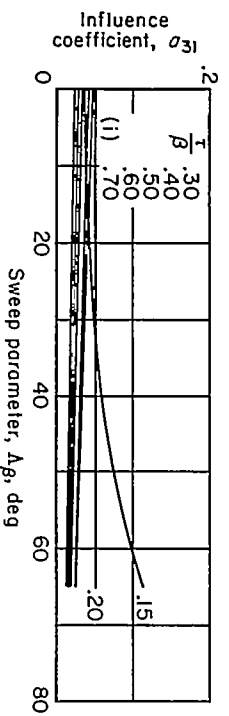
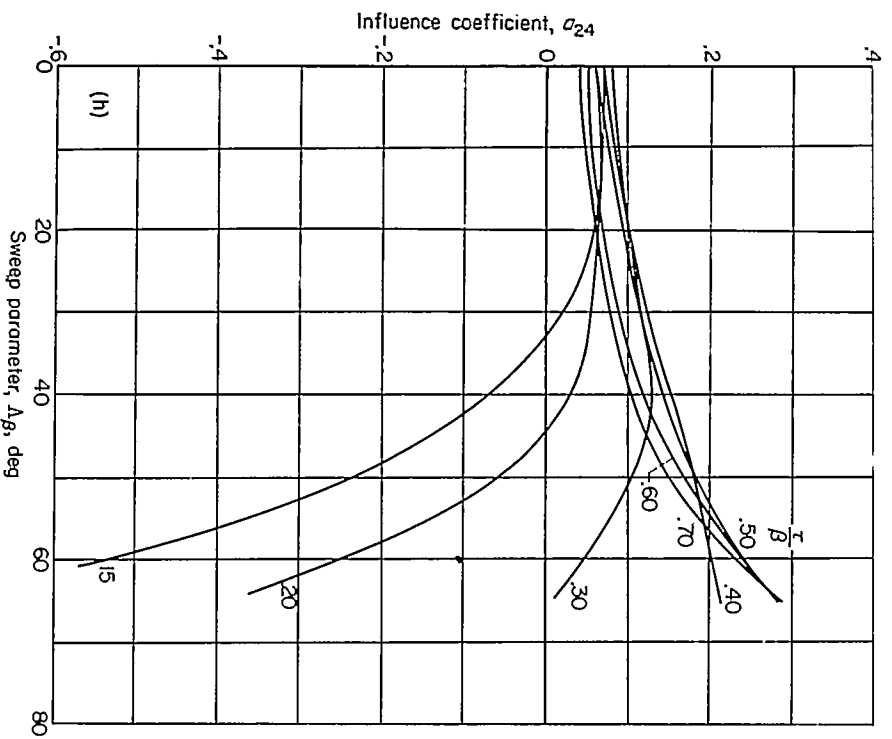


FIGURE 16.—Continued.

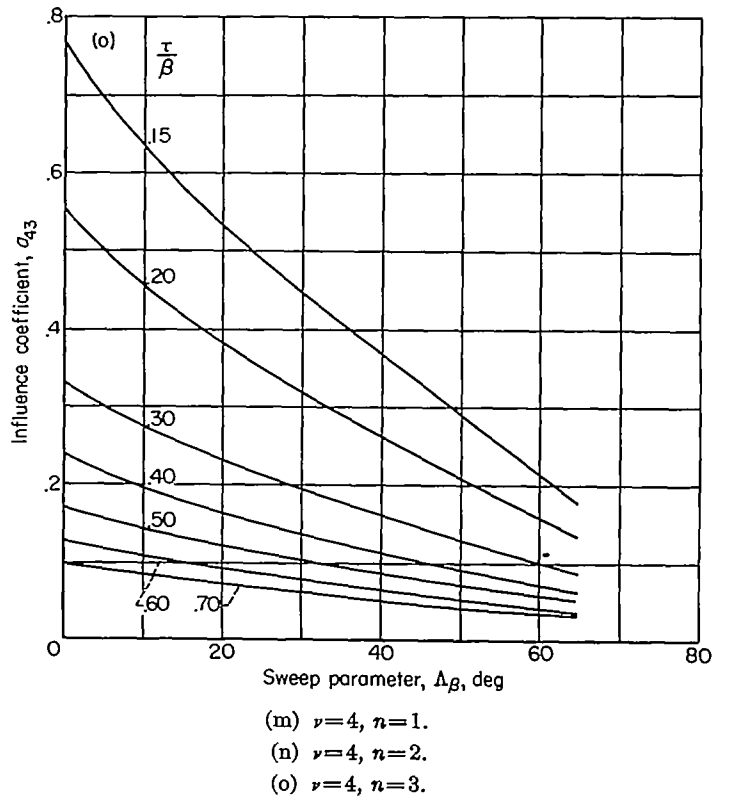
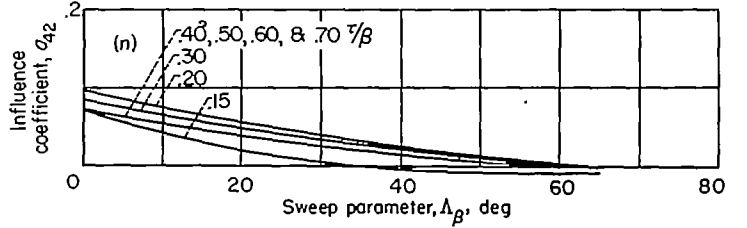
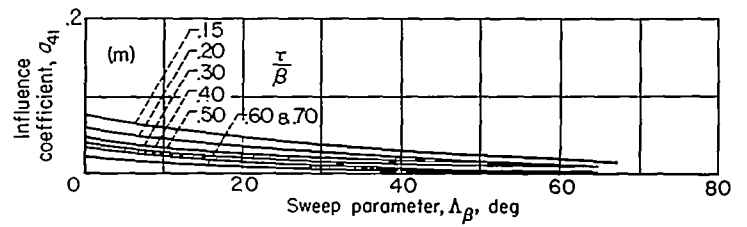
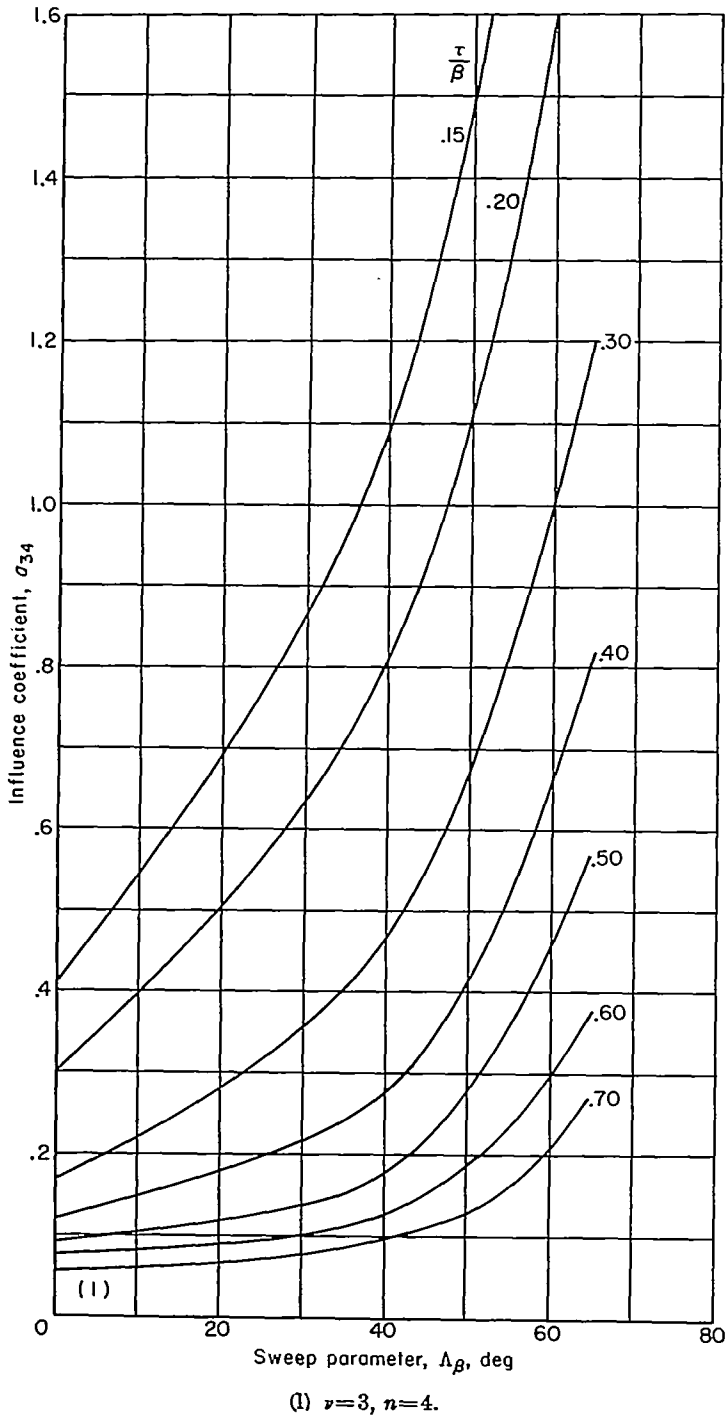
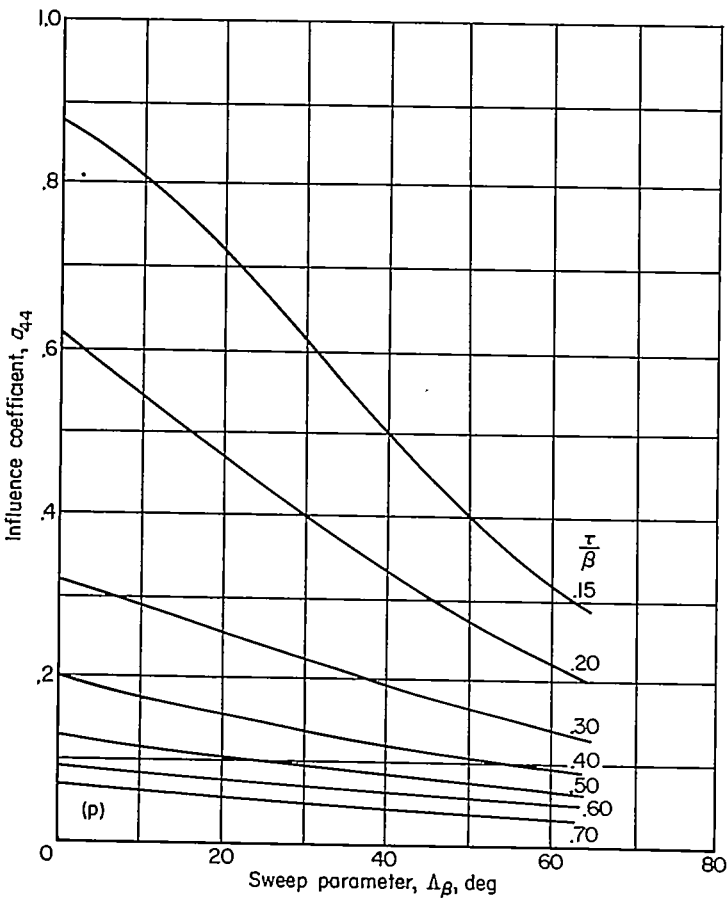


FIGURE 16.—Continued



(p) $\nu=4, n=4.$

FIGURE 16.—Concluded.

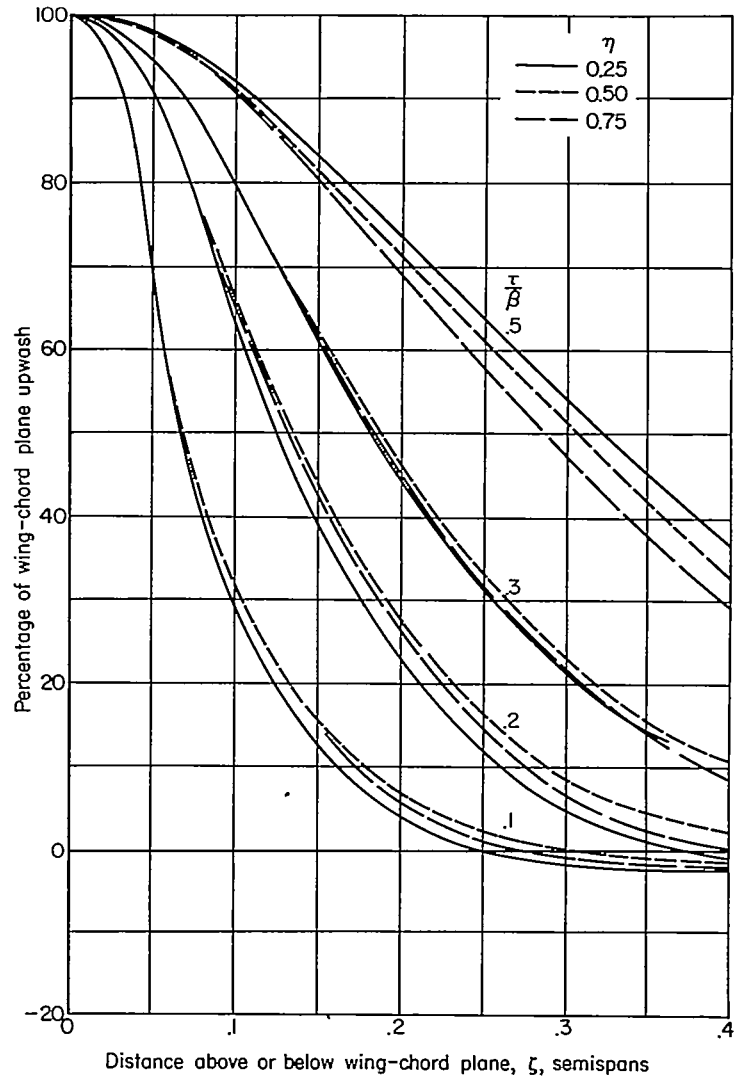


FIGURE 17.—Variation of upwash of a 40° swept-back horseshoe vortex with vertical position.

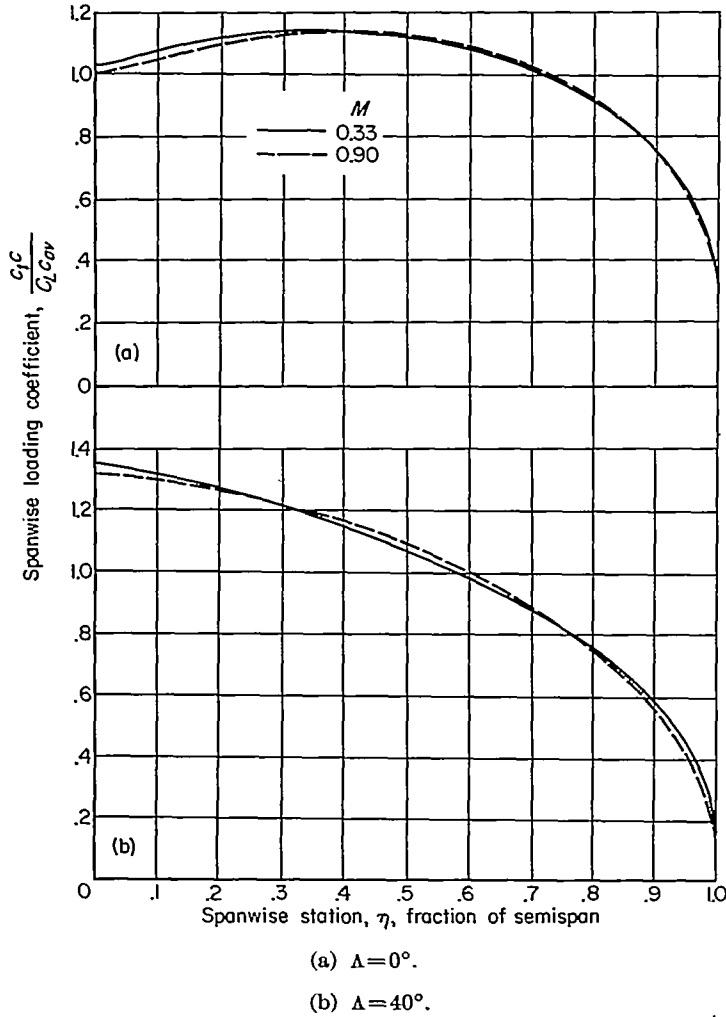


FIGURE 18.—A comparison of effects of compressibility on the spanwise loading coefficient for an unswept and a swept-back wing.

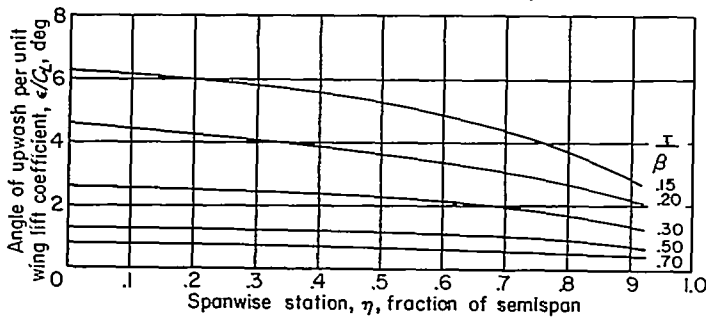


FIGURE 19.—The spanwise distribution of upwash at constant values of τ/β for an unswept wing at subsonic Mach numbers.

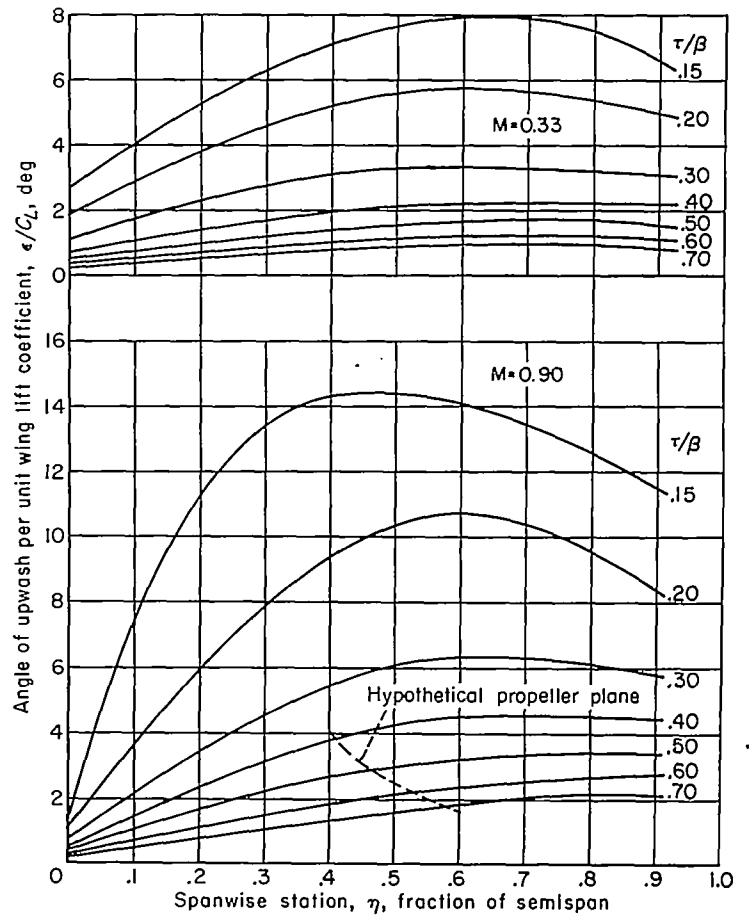


FIGURE 20.—The effects of compressibility on the spanwise distribution of upwash at constant values of τ/β for a wing swept back 40° .

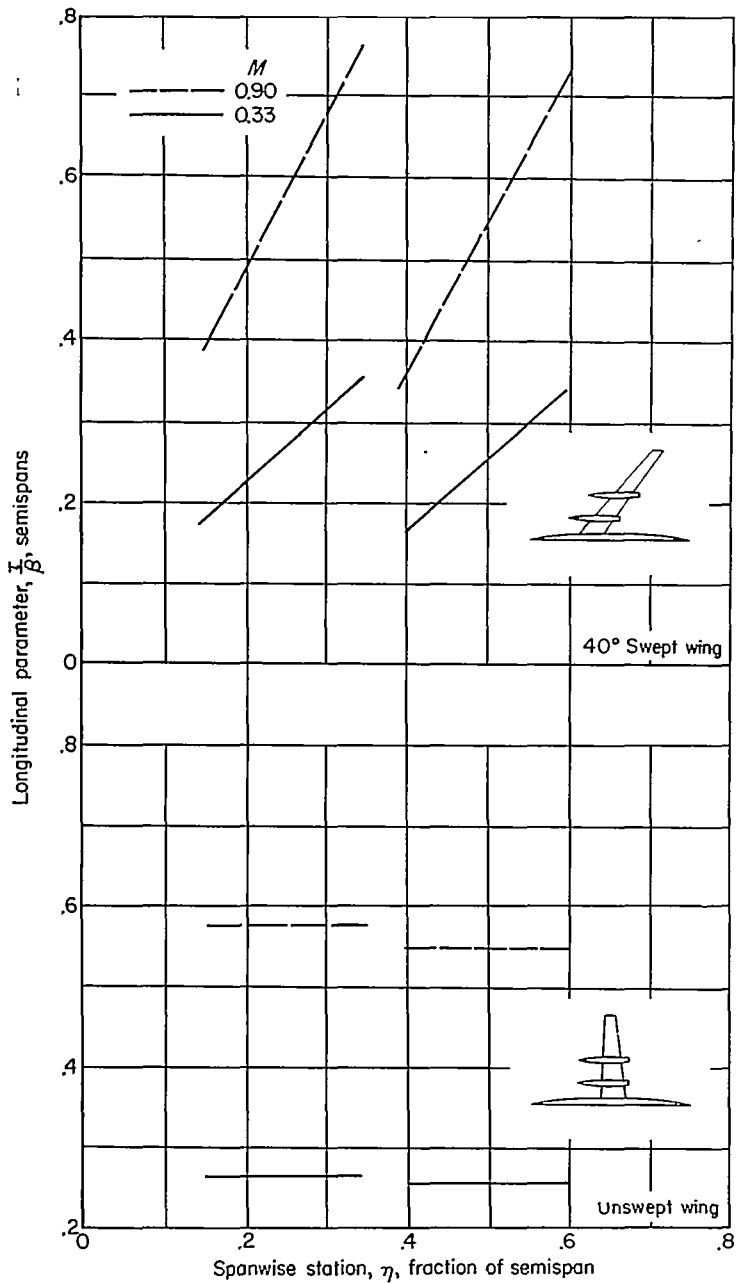


FIGURE 21.—The variation of the longitudinal parameter, τ/β , at the horizontal center line of the propeller disks of two hypothetical airplanes for a low- and a high-speed flight condition.

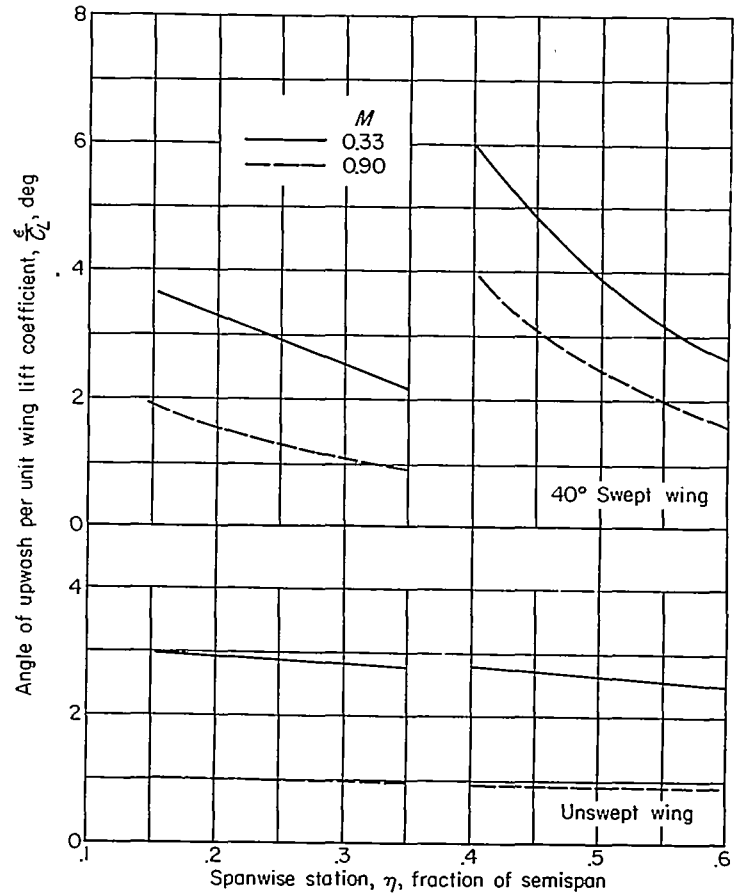


FIGURE 22.—The variation of the upwash angle at the horizontal center line of the propeller disks of two hypothetical airplanes for a low- and high-speed flight condition.

APPENDIX D

METHOD FOR COMPUTING THE BODY-INDUCED UPWASH ANGLES AT THE HORIZONTAL CENTER LINE OF A PROPELLER DISK

COMPUTATION OF THE UPWASH ANGLES AT THE HORIZONTAL PLANE OF SYMMETRY OF A BODY

A method was developed for calculating the upwash angles induced at the horizontal plane of symmetry of a finite body of revolution with radius which varies along the longitudinal axis.

The induced upwash at the horizontal plane of symmetry of a body of revolution is a result primarily of the displacement of the transverse flow about the body. The transverse velocity W (see fig. 1(b)) normal to the body center line results from the body being at an angle of attack to the free-stream velocity as shown in figure 1(b). The transverse

flow about an infinitely long cylinder may be obtained by covering the longitudinal axis of the cylinder with doublets of moment per unit length, μ (ref. 14). The potential function $d\Phi$ of a doublet element of strength μdx is

$$d\Phi = \frac{-\mu}{4\pi r'} \cos \Omega \sin \lambda d\lambda \tag{D1}$$

where

$$\lambda = \tan^{-1} \frac{r'}{x'}$$

r' distance along any radial line from the body longitudinal axis, ft

x' longitudinal distance from any doublet element on the body longitudinal axis to a transverse plane containing the point at which the upwash angle is to be computed, positive downstream from the doublet element, ft

The potential function Φ for a distribution of doublets along the longitudinal axis of a finite cylinder is obtained by integrating from the leading edge or most forward point (LE) to the trailing edge or most rearward point (TE) on the body.

$$\Phi = \frac{-\cos \Omega}{4\pi r'} \int_{\lambda_{LE}}^{\lambda_{TE}} \mu \sin \lambda \, d\lambda \quad (D2)$$

Differentiating equation (D2) with respect to Ω

$$\frac{d\Phi}{d\Omega} = \frac{\sin \Omega}{4\pi r'} \int_{\lambda_{LE}}^{\lambda_{TE}} \mu \sin \lambda \, d\lambda \quad (D3)$$

The expression for the velocity V_Ω tangential to a body of revolution and perpendicular to the transverse plane (see fig. 1(b)), is

$$V_\Omega = \frac{1}{r'} \frac{d\Phi}{d\Omega} \quad (D4)$$

Substituting the value of $d\Phi$ from equation (D3) in (D4)

$$V_\Omega = \frac{\sin \Omega}{4\pi (r')^2} \int_{\lambda_{LE}}^{\lambda_{TE}} \mu \sin \lambda \, d\lambda \quad (D5)$$

If a strength of $\mu = 2\pi R_b^2 W$ is assigned to each doublet representing a cylinder of constant radius R_b , equation (D5) yields the tangential velocity.

For a body of revolution whose radius varies with position along the longitudinal axis, it was considered that each transverse section was a section of an infinitely long cylinder with radius equal to that at the section. The doublet strength μ was allowed to vary as R_b^2 . For this case, the equation for the tangential velocity V_Ω becomes

$$V_\Omega = \frac{\sin \Omega V_\infty \sin \alpha}{2(r')^2} \int_{\lambda_{LE}}^{\lambda_{TE}} R_b^2 \sin \lambda \, d\lambda \quad (D6)$$

When α and ϵ are small angles, the upwash angle in the horizontal plane for $\Omega = 90^\circ$ is (see fig. 1(b))

$$\epsilon = \frac{V_\Omega}{V_\infty} = \frac{\alpha}{2(r')^2} \int_{\lambda_{LE}}^{\lambda_{TE}} R_b^2 \sin \lambda \, d\lambda \quad (D7)$$

As has been shown by Munk and von Kármán, for calculations of potential flow in the vicinity of the nose of a body, variations in the body radius need be considered only over the forward half-body. The body downstream of the midsection can be assumed to continue to infinity with a radius equal to that at the midsection. Therefore, the upper limit λ_{TE} can be assumed to be π . The integration is accomplished numerically to the midsection, after which the integral becomes a simple one because of the assumed constant radius.

The expression in equation (D7) is for closed bodies of revolution. For bodies through which there was air flow, in applying the equation the surface was considered to close across the openings as if there were no through flow.

It is realized that the axial component of velocity is somewhat increased over the free-stream velocity because of the variation in body shape along the longitudinal axis. However, these increases are only a small percentage of V_∞ and, therefore, they have been neglected. Similarly, a radial flow is induced by the body shape variation, but since it does not enter into the computation of ϵ at the horizontal plane of symmetry, it has been ignored.

Minor asymmetries in body shape downstream of the propeller plane were found to have little effect on the upwash angles induced at the propeller plane. This will be demonstrated during the evaluation of the method. If the body was not symmetrical in the longitudinal vertical plane, it was found satisfactory to use the mean thickness line of the body when determining the effective angle of attack.

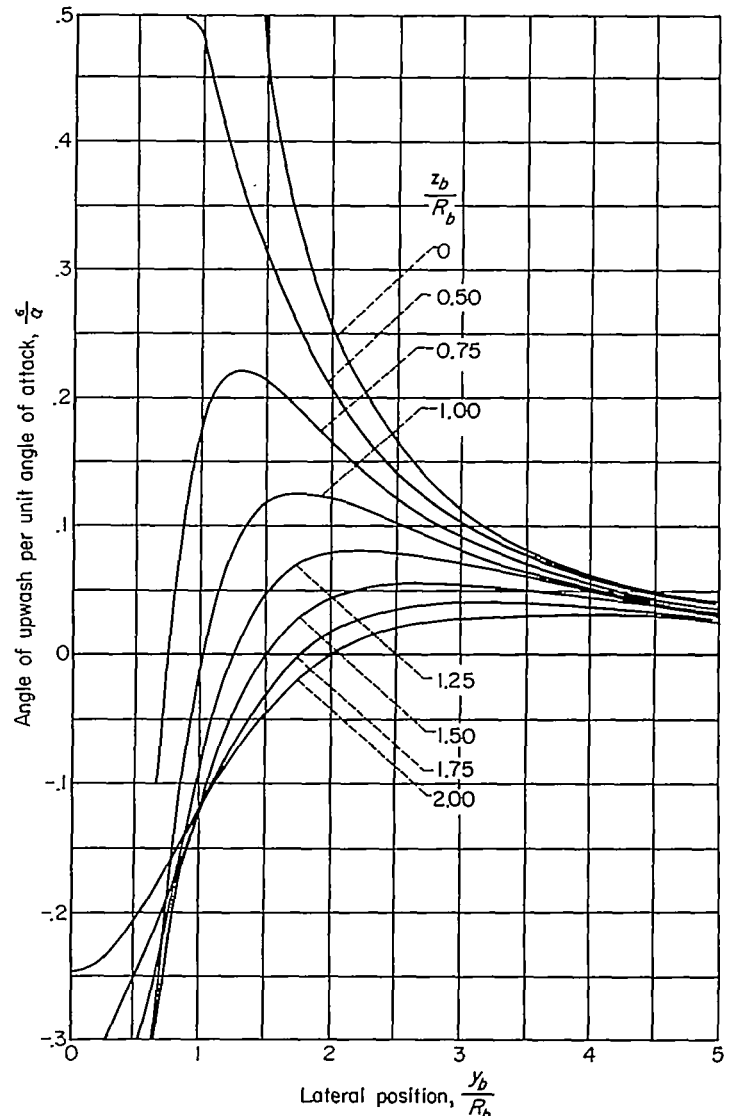


FIGURE 23.—The variation of upwash angle with vertical position in a transverse plane for an infinite cylinder.

EXTENSION OF THE METHOD TO POSITIONS ABOVE AND BELOW THE HORIZONTAL PLANE OF SYMMETRY

For angular positions other than the horizontal plane of symmetry of a body, the upwash is no longer a function of the induced tangential velocity only, but is also affected by the induced radial velocity. To obtain the upwash at positions other than the horizontal plane of symmetry for a finite body of varying radius is a difficult task for which there is, at present, no adequate solution. On the other hand, the upwash at any point about an infinite cylinder in incompressible flow may be obtained quite easily. The value of ϵ induced by an infinite cylinder at any point defined by the lateral and vertical distances from the body center line, y_b and z_b , for small values of α may be determined as

$$\epsilon_{y_b, z_b} = \frac{\Delta W}{V_\infty} = \alpha \left\{ \frac{(y_b/R_b)^2 - (z_b/R_b)^2}{[(y_b/R_b)^2 + (z_b/R_b)^2]^2} \right\} \quad (D8)$$

Variations of ϵ per unit angle of attack versus lateral position y_b for several vertical positions z_b are shown in figure 23.

EVALUATION OF THE METHOD

The method was applied at the horizontal plane of symmetry of three bodies where the horizontal center line of the propeller disk was coincident with the horizontal plane of symmetry. The models were tested in the Ames 40- by 80-foot wind tunnel at a Mach number of 0.18 to obtain experimental values of the upwash angles (ref. 5). The geometric characteristics of the models are shown in figure 24. Figure 25 shows comparisons of the experimental and computed upwash angle distributions. Good agreement is apparent.

A fourth body, which was not symmetrical in the longitudinal-vertical plane, was tested in the Ames 12-foot wind tunnel (ref. 9) through a Mach number range from 0.33 to 0.92. The geometric characteristics of the body are shown in figure 26. Computations were made for this body assuming the plane of symmetry to be that of the forebody and ignoring the asymmetry downstream. The comparisons shown in figure 27 at the lower Mach numbers indicate that the asymmetry had little effect on the accuracy of the computations. The measured and computed values do not agree beyond a Mach number of 0.6. These differences are believed due to the onset of compressibility effects which have not been taken into account in the computations.

An indirect evaluation of the extension of the method above and below the horizontal plane of symmetry is shown by the results of the computations of total upwash angles for complete wing-nacelle-fuselage configurations as shown in Appendix B.

Nacelle coordinates			
Station	Radius	Station	Radius
0	21.5	42	29.7
1	23.0	48	29.8
2	24.0	54	29.8
4	25.0	62	29.8
6	26.0	72	29.8
9	27.0	96	29.5
12	27.8	120	29.0
18	28.5	144	26.5
24	29.0	168	22.4
30	29.5	192	16.4
36	29.6	217	11.2

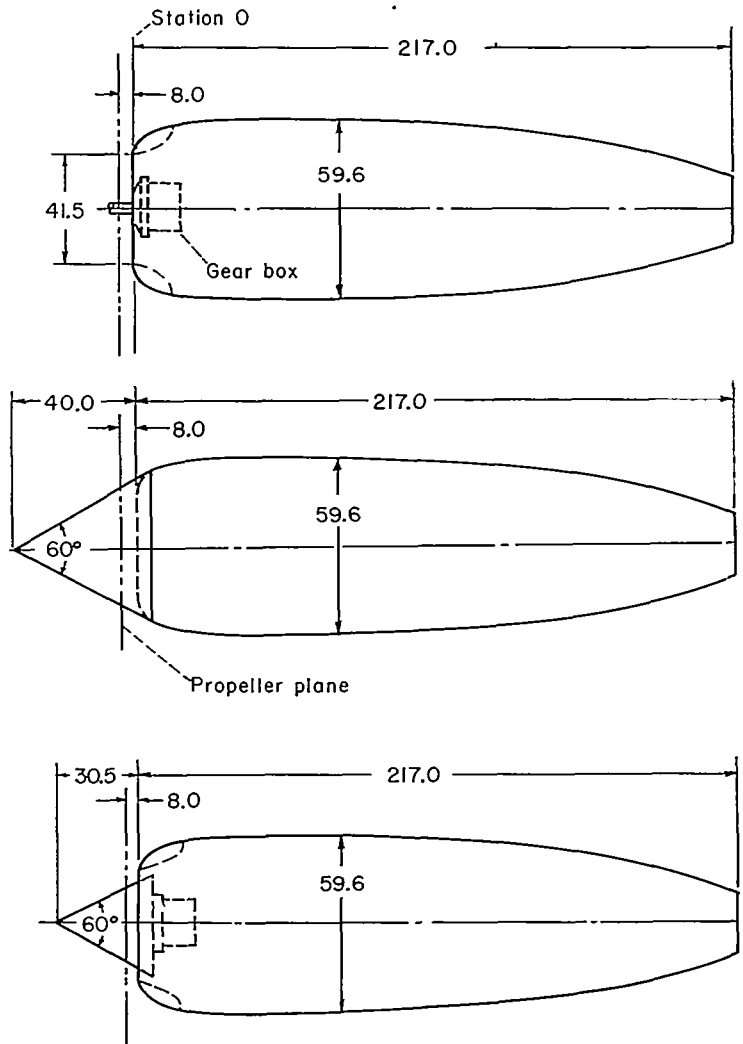


FIGURE 24.—Geometric characteristics of three nacelles tested at $M=0.18$. All dimensions are in inches.

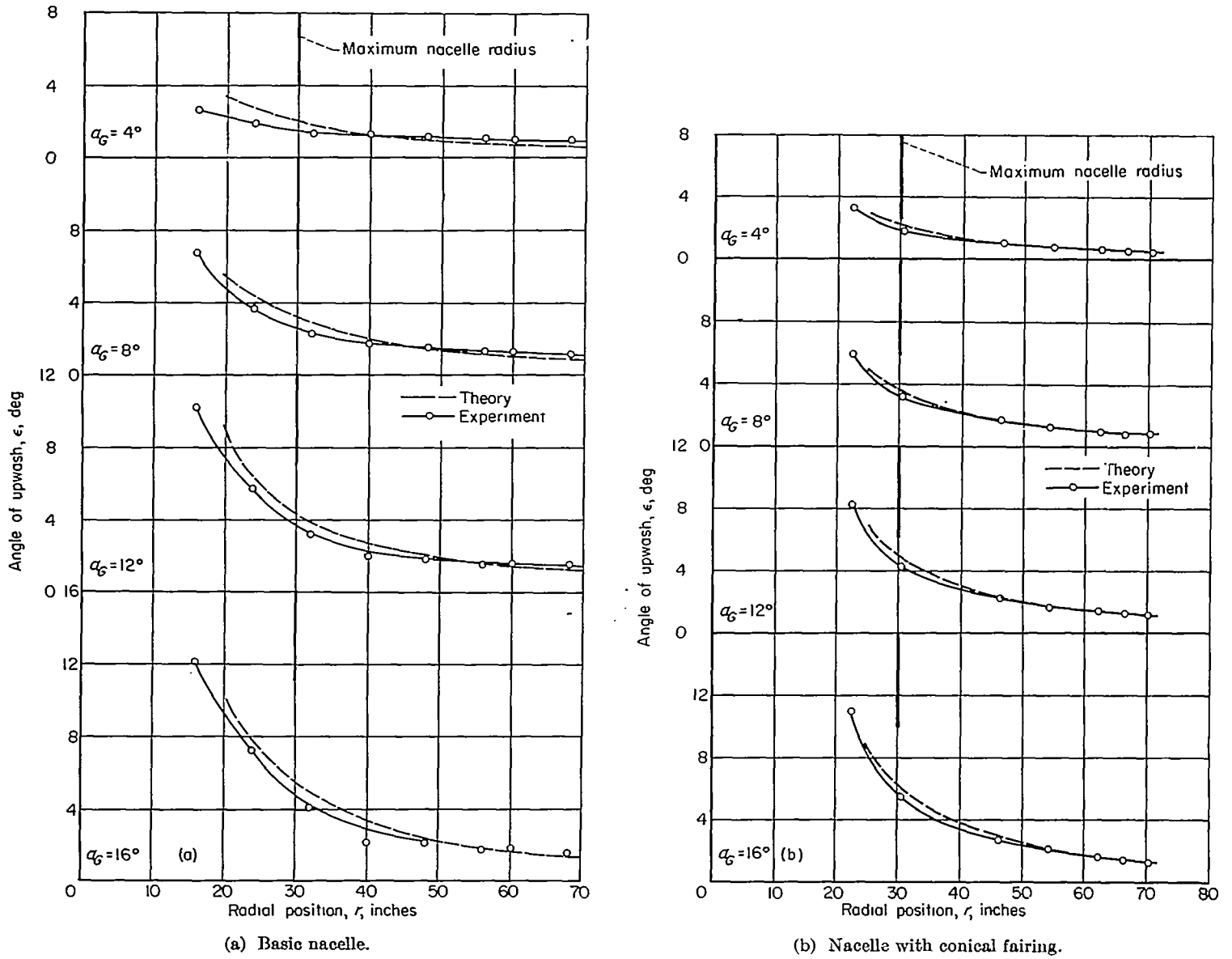
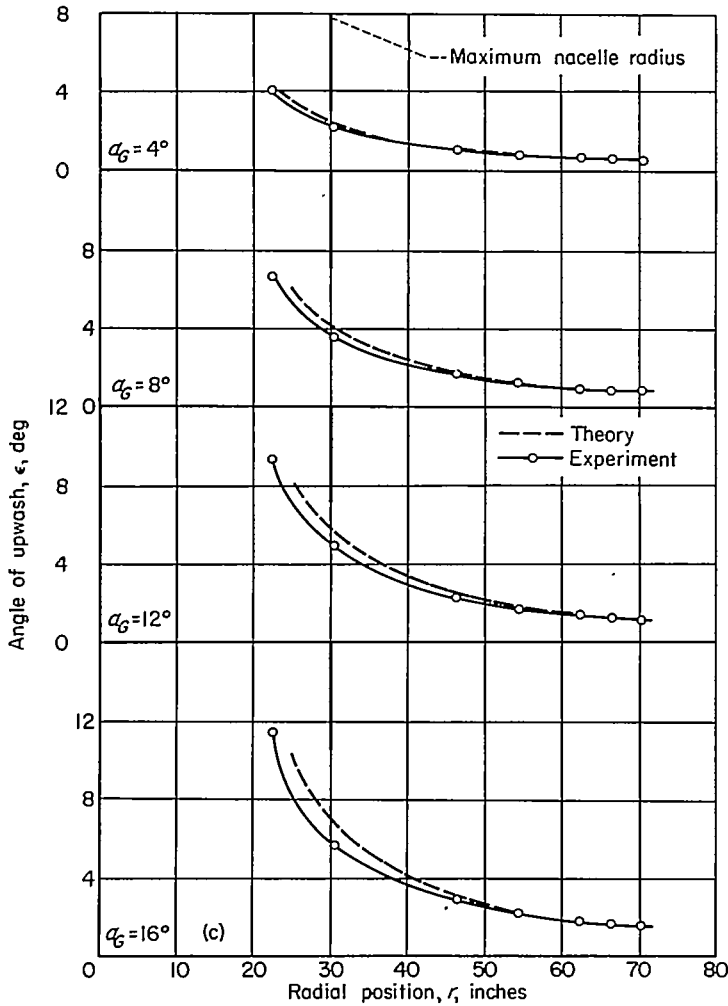


FIGURE 25.—Comparison of measured and computed variations of the angle of upwash at the horizontal center line of the propeller disk. $M=0.18$.



(c) Nacelle with conical spinner.

FIGURE 25.—Concluded.

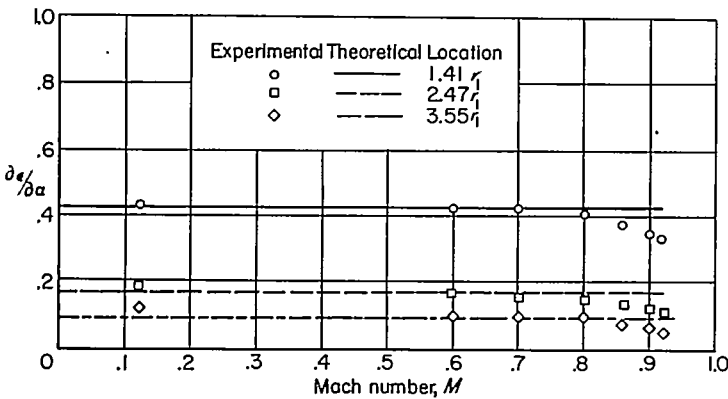


FIGURE 27.—The effects of Mach number on the upwash parameter $\partial\epsilon/\partial\alpha$ for an isolated nacelle.

Nacelle coordinates			
Sta	r_1	Sta	r_2
-5.00	0	2.00	0.350
-4.79	.385	3.00	.419
-4.58	.567	4.00	.616
-4.25	.788	5.00	.919
-3.95	.951	6.00	1.290
-3.25	1.242	7.00	1.685
-2.55	1.472	8.00	2.056
-1.80	1.670	9.00	2.359
-.80	1.871	10.00	2.556
0	1.985	11.00	2.625
2.00	2.100	30.50	2.625
12.00	2.100	32.50	2.450
		34.50	2.220
		36.50	1.825
		38.50	1.270
		40.50	.675
		41.50	.275
		42.25	0

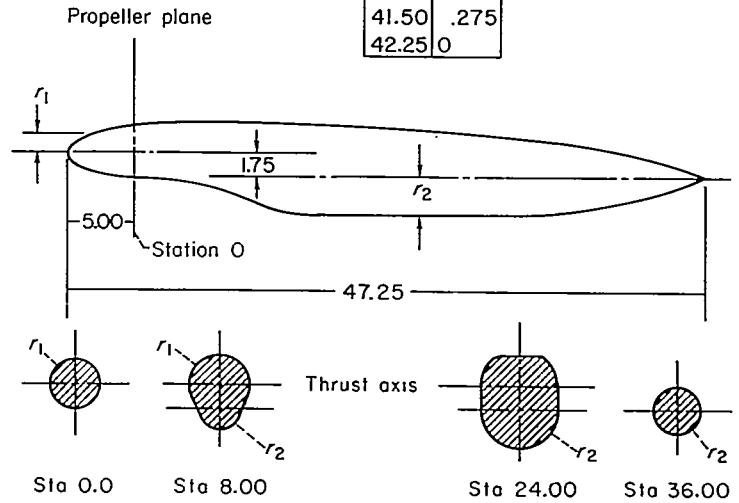


FIGURE 26.—Geometric characteristics of nacelle tested from Mach number of 0.33 to 0.92. All dimensions are in inches.

REFERENCES

1. Vogeley, A. W.: Calculation of the Effect of Thrust-Axis Inclination on Propeller Disk Loading and Comparison with Flight Measurements. NACA TN 1721, 1948.
2. Gray, W. H., Hallissy, J. M., Jr., and Heath, A. R.: A Wind-Tunnel Investigation of the Effects of Thrust-Axis Inclination on Propeller First-Order Vibration. NACA Rep. 1205, 1954.
3. Roberts, John C., and Yaggy, Paul F.: A Survey of the Flow at the Plane of the Propeller of a Twin-Engine Airplane. NACA TN 2192, 1950.
4. Rogallo, Vernon L., Roberts, John C., and Oldaker, Merritt R.: Vibratory Stresses in Propellers Operating in the Flow Field of a Wing-Nacelle-Fuselage Combination. NACA TN 2308, 1951.
5. Yaggy, Paul F.: A Method for Predicting the Upwash Angles Induced at the Propeller Plane of a Combination of Bodies with an Unswept Wing. NACA TN 2528, 1951.
6. Rogallo, Vernon L.: Effects of Wing Sweep on the Upwash at the Propeller Planes of Multiengine Airplanes. NACA TN 2795, 1952.

7. Rogallo, Vernon L., and McCloud, John L., III: Calculations of Upwash in the Region Above or Below the Wing-Chord Planes of Swept-Back Wing-Fuselage-Nacelle Combinations. NACA TN 2894, 1953.
8. Rogallo, Vernon L., and McCloud, John L., III: Survey of the Flow Fields at the Propeller Planes of Six 40° Sweptback Wing-Fuselage-Nacelle Combinations. NACA TN 2957, 1953.
9. Lopez, Armando E., and Dickson, Jerald K.: The Effects of Compressibility on the Upwash at the Propeller Planes of a Four-Engine Tractor Airplane Configuration Having a Wing With 40° of Sweepback and an Aspect Ratio of 10. NACA TN 3675, 1956.
10. Stulen, F. B., and DeVries, J. A.: Calculation of the First-Order Vibratory Propeller Blade Stresses by the Integration or Simplified Matrix Method. Rep. No. C-2132, Propeller Division, Curtiss-Wright Corp., Jan. 27, 1950.
11. Glauert, H.: The Elements of Aerofoil and Airscrew Theory. Second ed., Ch. XII, the University Press, Cambridge, England, 1947.
12. DeYoung, John, and Harper, Charles W.: Theoretical Symmetric Span Loading at Subsonic Speeds for Wings Having Arbitrary Plan Form. NACA Rep. 921, 1948.
13. Spreiter, John R., and Sacks, Alvin H.: The Rolling Up of the Trailing Vortex Sheet and Its Effect on the Downwash Behind Wings. Jour. Aero. Sci., vol. 18, no. 1, Jan. 1951, pp. 21-32.
14. von Kármán, Theodor: Calculation of Pressure Distribution on Airship Hulls. NACA TM 574, 1930.